Cerebral Cortex, August 2016;26: 3508–3526

doi:10.1093/cercor/bhw157
Advance Access Publication Date: 26 May 2016
Original Article

ORIGINAL ARTICLE

The Human Brainnetome Atlas: A New Brain Atlas Based on Connectional Architecture

Lingzhong Fan[1], Hai Li[1,2], Junjie Zhuo[4], Yu Zhang[1,2], Jiaojian Wang[4], Liangfu Chen[1,2], Zhengyi Yang[1,2], Congying Chu[1,2], Sangma Xie[1,2], Angela R. Laird[10], Peter T. Fox[7], Simon B. Eickhoff[8,9], Chunshui Yu[6] and Tianzi Jiang[1,2,3,4,5]

[1]Brainnetome Center, [2]National Laboratory of Pattern Recognition and, [3]CAS Center for Excellence in Brain Science and Intelligence Technology, Institute of Automation, Chinese Academy of Sciences, Beijing 100190, China, [4]Key Laboratory for NeuroInformation of the Ministry of Education, School of Life Science and Technology, University of Electronic Science and Technology of China, Chengdu 625014, China, [5]The Queensland Brain Institute, University of Queensland, Brisbane, QLD 4072, Australia, [6]Department of Radiology, Tianjin Medical University General Hospital, Tianjin, China, [7]Research Imaging Institute, University of Texas Health Science Center, San Antonio, TX, USA, [8]Institute of Neuroscience and Medicine (INM-1), Research Centre Juelich, Juelich 52425, Germany, [9]Institute for Clinical Neuroscience and Medical Psychology, Heinrich-Heine-University Düsseldorf, Düsseldorf 40225, Germany and [10]Department of Physics, Florida International University, Miami, FL, USA

Address correspondence to Tianzi Jiang, Brainnetome Center, Institute of Automation, Chinese Academy of Sciences, Beijing 100190, China. Email: jiangtz@nlpr.ia.ac.cn

Lingzhong Fan and Hai Li equally contributed to this work.

Abstract

The human brain atlases that allow correlating brain anatomy with psychological and cognitive functions are in transition from ex vivo histology-based printed atlases to digital brain maps providing multimodal in vivo information. Many current human brain atlases cover only specific structures, lack fine-grained parcellations, and fail to provide functionally important connectivity information. Using noninvasive multimodal neuroimaging techniques, we designed a connectivity-based parcellation framework that identifies the subdivisions of the entire human brain, revealing the in vivo connectivity architecture. The resulting human Brainnetome Atlas, with 210 cortical and 36 subcortical subregions, provides a fine-grained, cross-validated atlas and contains information on both anatomical and functional connections. Additionally, we further mapped the delineated structures to mental processes by reference to the BrainMap database. It thus provides an objective and stable starting point from which to explore the complex relationships between structure, connectivity, and function, and eventually improves understanding of how the human brain works. The human Brainnetome Atlas will be made freely available for download at http://atlas.brainnetome.org, so that whole brain parcellations, connections, and functional data will be readily available for researchers to use in their investigations into healthy and pathological states.

Key words: brain atlas, connectivity-based parcellation, diffusion tensor imaging, functional characterization, resting-state functional connectivity

Introduction

The human brain contains hundreds of anatomically and functionally distinct cortical and subcortical structures, accurately defining these parcellations and mapping their functions and connections pose massive challenges. However, a reliable brain atlas reflecting this subdivision is essential to quantitatively investigate the functional and structural characteristics of the human brain. Such an atlas would then allow brain network analyses in an informed way using a priori defined nodes rather than resorting to arbitrary brain divisions or using data-driven parcellations specific to the specific subjects at hand (de Reus and van den Heuvel 2013; Sporns 2015). In addition, it would also offer a powerful framework for synthesizing the results of different imaging studies (Devlin and Poldrack 2007; Van Essen 2013; Amunts et al. 2014).

Consequently, there has been a long-standing effort to parcellate the brain into areas based on microstructural, macrostructural, or connectional features (Toga et al. 2006; Amunts and Zilles 2015). Early parcellation efforts aimed at defining regional boundaries, including the widely used Brodmann atlas, relied on postmortem architecture using limited samples (Brodmann 1909; Zilles and Amunts 2010). Although such atlases have provided invaluable information, their microscale cytoarchitectonics is insufficient to completely represent brain organization (Van Essen 2013). In particular, microstructural heterogeneity represents only one aspect of cortical differentiation, namely, local features, while being insensitive to the second major determinant of regional specialization, that is, heterogeneity in long-range connections (Passingham et al. 2002). Although histological examination is currently the only technique that actually maps the brain directly (rather than inferring parcellations from recorded data), systematic cytoarchitectonical mapping procedures are extremely time-consuming and must be complemented by information on the heterogeneity of connectivity patterns.

In the past 2 decades, information gained from advanced brain mapping technologies, in particular multimodal magnetic resonance imaging (MRI), including structural, functional, and diffusion MRI, has offered alternative ways to tackle the challenge of cortical cartography (Behrens et al. 2003; Johansen-Berg et al. 2004; Cohen, Fair, et al. 2008; Cohen, Lombardo, et al. 2008; Kim et al. 2010; Eickhoff et al. 2011). Most of these still rapidly developing approaches are based on the aforementioned concept that each cortical area has a unique pattern of inputs and outputs (a "connectional fingerprint"), which, together with the local infrastructure provided by microstructural properties as mentioned above, represent the second major determinant of the function of that area (Passingham et al. 2002). Therefore, the basic idea of connectivity-based parcellation is to suppose that those voxels belonging to a given brain area share similar connectivity profiles. In turn, brain areas should thus be definable by aggregating voxels showing similar connectivity patterns into larger clusters. A considerable number of studies have already used connectivity-based parcellations to form cartographic maps of specific regions of the brain or even the entire cortex (Eickhoff et al. 2015); however, there are several inconsistencies between them and in particular a whole-brain parcellation scheme based on structural connectivity information is still missing.

The Brainnetome Project was launched to investigate the hierarchy in the human brain from genetics to neuronal circuits to behaviors (Jiang 2013), conceptualizing 2 components (nodes and connections) as the basic research unit. One of the key prerequisites of this project is thus to establish a new human brain atlas, that is, the Brainnetome Atlas, defining these nodes based on structural connectional architecture. Importantly, the Brainnetome Atlas should follow the concept of a multimodal characterization providing not only fine-grained subregions based on structural connectivity patterns but complement these by detailed functional connectivity patterns for each area. Furthermore, mapping cognitive processes onto these modules is central to understanding the functional organization of the human brain and hence a comprehensive structure-to-function mapping of the subregions forming the Brainnetome Atlas should likewise be performed. Together these types of information would then establish a new framework for the allocation of activations and the investigation of whole-brain connectivity matrices. This article describes the current progress in forming this new human brain atlas based on connectional architecture and its ability to link brain connectivity to function, which together could help reveal the neurophysiological substrates of various diseases and cognitive functions.

Materials and Methods

Subjects and Data Acquisitions

Data from 40 healthy, unrelated adults (age: 22–35, 17 males) were obtained from the Q3 data release from the Human Connectome Project (HCP) database. The multimodal MRI data consisted of structural MRI, resting-state functional MRI (rfMRI), and diffusion MRI (dMRI), collected on a 3 T Skyra scanner (Siemens, Erlangen, Germany) using a 32-channel head coil. Because subjects 209 733 and 528 446 displayed structural brain abnormalities, they were replaced by 2 other subjects, 100 408 and 106 016, from the unrelated 80 subjects' group. All scanning parameters are detailed and motivated in Van Essen et al. (2013) and also provided in the supplement. Multimodal MRI data from the database were downloaded in a preprocessed form, that is, after the images had undergone the minimal preprocessing pipeline (v. 3.2). The details of this pipeline have been described previously (Jenkinson et al. 2002, 2012; Glasser et al. 2013; Smith et al. 2013) and are only summarized in the supplement for completeness.

In addition, another independent group of healthy subjects were included to do the repeatability validation. The dataset included 40 (20 males, age range, 17–20 years, age, 19.10 ± 0.80 years, mean ± SD) right-handed participants. The multimodal MRI data of 40 healthy adults were acquired using a 3.0 T GE MR Scanner (see Zhuo et al. (2016) for a full description of the data sample and acquisition parameters).

Initial Seed Masks Definition

First, each subject's T_1 image was parcellated into 34 cortical regions of interest (ROIs) per hemisphere and 14 subcortical ROIs based on the Desikan–Killiany (DK) atlas (Desikan et al. 2006). We then combined ROIs representing (arbitrary) subdivisions of a larger gyrus as well as those whose boundaries are determined

by sulci that are highly variable (cf. Supplementary Table 1). In addition, we combined the basal ganglia into a single region of interest for subsequent parcellation (Tziortzi et al. 2014). The full name and abbreviation of each initial cortical and subcortical seed mask are listed in Supplementary Table 1. All the cortical and subcortical volumetric ROIs were extracted in MNI space based on the preprocessed individual structural data. These initial seed masks in each subject were then used to create population probability maps that were binarized using a threshold of 25% to obtain the volumetric ROIs. These ensuing masks were used as a starting point for the connectivity-based parcellation analysis (Fig. 1A).

Probabilistic Diffusion Tractography

The (HCP minimally preprocessed) diffusion MRI data were further processed using the FMRIB Diffusion Toolbox. First, fiber orientation and associated uncertainties in each voxel were estimated using FSL's BEDPOSTX algorithm, estimating probability distributions for multiple fiber directions at each voxel (Behrens et al. 2007). Second, skull-stripped T_1-weighted images for each subject were co-registered to the subject's non-diffusion-weighted image ($b = 0$ s/mm^2). On the basis of these aligned T_1 images, we derived (forward and inverse) nonlinear transformations between the diffusion space and the MNI 152

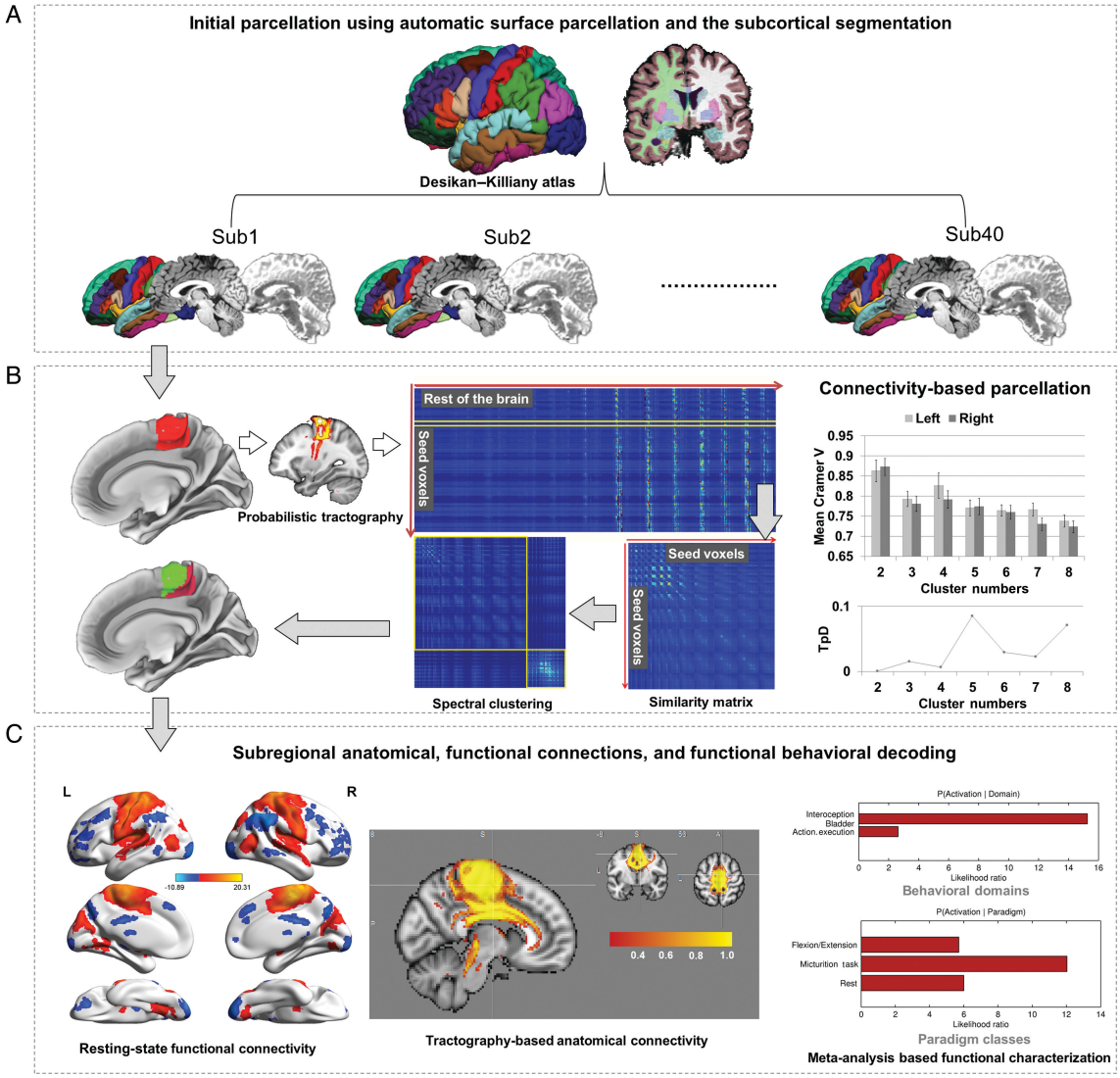

Figure 1. Framework of the Brainnetome Atlas construction based on connectivity-based parcellation. (*A*) Initial parcellation using automatic surface parcellation and subcortical segmentation. The FreeSurfer DK atlas produced the initial parcellations based on gyri and sulci. (*B*) Tractography-based parcellation with in vivo connectional architecture. Taking the parcellation of the human paracentral lobule by diffusion tensor imaging as an example, the paracentral lobule was first extracted from the DK atlas. The connectional architecture was then mapped with probabilistic tractography using diffusion MRI, after which, by calculating the similarity/dissimilarity between the connectivity architecture, the paracentral lobule was divided into subregions with distinguishing anatomical connectivity patterns. The stability across the population and the interhemispheric anatomic homology were evaluated to determine the final cluster number. (*C*) Subregional anatomical and functional connections and functional behavioral decoding. Diffusion MRI combined with tractography was used to reconstruct the major fiber bundles, while functional connectivity analysis of resting-state functional MRI was used to provide the in vivo large-scale connectivity in the human brain. We also mapped the functions to each paracentral lobule subregion via the behavioral domain and paradigm analysis using the BrainMap Database.

structural template, which were then used to transform the seed masks into the diffusion space for each subject. We checked the registration accuracy of each seed region in the coronal, axial, and sagittal planes slice-by-slice in native diffusion space and manually modified the masks following the DK protocol (Desikan et al. 2006) where necessary. Then, the probabilistic tractography was applied by sampling 5000 streamline fibers for each voxel in the seed region to estimate its whole-brain connectivity profile. A small threshold value was then used to remove connectivity information of voxels that were only reached by no more than 2/5000 samples and hence most likely represent stray connectivity, that is, noise (Heiervang et al. 2006; Johansen-Berg et al. 2007; Makuuchi et al. 2009).

Connectivity-Based Parcellation Through Tractography

To facilitate data storage and analysis, the whole-brain connectivity profiles for each voxel were down-sampled to 5 mm isotropic voxels. Cross-correlation matrices between the connectivity patterns of all the voxels in the seed mask were calculated and used for automatic parcellation (Johansen-Berg et al. 2004). The cross-correlation matrix was then permutated using spectral clustering to define distinct clusters (Liu et al. 2013; Fan et al. 2014). Importantly, the number of clusters must be defined by the experimenter when using this method. In the current study, we explored parcellations from 2 up to 12 (depending on the size of the seed region) clusters (Fig. 1*B*; see Supplementary Figs 2–7). All (per subject) solutions were transformed into the MNI template space using the nonlinear transformations described above.

Owing to the random labeling of clusters by clustering algorithm across subjects, we try to find the most consistent labeling scheme across subjects by the following steps. First, the labeling schemes of each subject's clusters were pooled into a thresholded group-level cross-correlation matrix where each entry represents the connectional similarity of any 2 voxels in the ROI (Zhang et al. 2015). Then, the spectral clustering algorithm was applied again on this similarity matrix, and a group-level labeling scheme was, thus, yielded. Last, the labeling pattern was propagated back to each subject's clusters by maximization of spatial overlap using Munkres' assignment algorithm (Munkres 1957). We then calculated probabilistic maps representing the overlap of these clusters across the subjects and hence interindividual variability. Further, a maximum probability map (MPM) across all the subjects was created for each solution (number of clusters) by assigning each voxel to the most likely cluster at this position (Eickhoff et al. 2005). In addition, if 2 parcels representing the same region across hemispheres are given, the consistent labeling pattern across hemispheres is also achieved before propagation of the labeling pattern.

Determination of the Optimal Clustering Solution *K*

To avoid arbitrarily choosing the number of clusters, we used cross-validation to determine the number of clusters that yielded the optimal consistency across the subjects. We considered 2 general strategies for defining the optimized cluster number, that is, stability across the population and interhemispheric consistency of topographic arrangement (Fig. 1*B*; see Supplementary Figs 2–7).

The suitable number of subregions was first assessed by evaluating the reproducibility of the parcellation across random-split half sets as measured by Cramer's V (Liu et al. 2013; Fan et al. 2014). Participants were divided into 2 random groups, and the MPMs of the 2 randomly assembled groups were evaluated. The random-split half was then repeated 100 times to compute the average (and standard deviation) consistency. The optimal *K* was defined by the (local) peak of Cramer's V, indicating a better split-half reproducibility than the surrounding solutions.

We also evaluated the topological distance (TpD) to quantify the similarity in topological arrangement of putatively homologous areas on either hemisphere (Tungaraza et al. 2015). To this end, we computed a $K \times K$ topology matrix for a given parcellation. The (i, j) entry of this matrix was the number of voxels from region i that were spatially in contact (26-nearest neighbor) with voxels from region j. The TpD between the left and right given subregions in each hemisphere was defined as the cosine distance of the 2 matrices (normalized to a sum of 1 and vectorized), yielding TpD scores that range from 0 (identical topology) to 1 (completely incongruent topology).

Mapping Anatomical Connectivity Patterns

To map the whole-brain anatomical connectivity pattern for each subregion of the atlas, we performed probabilistic tractography by drawing 5000 samples from each voxel in each subregion (thresholded at 25% probability) to all the other voxels of the whole brain. To reduce the noise in fiber tracking, the raw trace counts for each subject were thresholded at a trace count of ≥2. Next, we obtained a population map of the major fiber bundles for each subregion by binarizing the obtained per-subject tractograms, normalizing them into standard space, computation of a probabilistic fiber-tract map, and thresholding the latter at 50% probability. In addition, we also computed the structural connectome between all identified subregions, again binarized them using a threshold for stray connectivity of ≥2 and then employed a nonparametric 1-tailed sign test to determine the connections that are consistent across subjects (Gong et al. 2009). To reduce the chances of obtaining false-positive connections, a Bonferroni correction was used to adjust for multiple comparisons (i.e., 246 × 245/2 = 30 135 pairs of subregions) at $P < 0.001$.

Mapping Resting-State Functional Connectivity Patterns

To map the whole-brain resting-state connectivity pattern for each atlas subregion, we resampled each subregion (thresholded at 50% probability) at the 2 mm resolution of the resting-state data and computed its average time series per subject. A functional connectivity map was then provided by the Pearson's correlation coefficient between the mean time series of each subregion and that of each voxel in the whole brain. The obtained correlation coefficients were normalized using Fisher's z-transformation and tested for statistical significance on the group level using a 1-sample *t* tests (FDR corrected inference at $P < 0.05$ with an additional extent-threshold of 50 voxels).

Function Decoding Using the BrainMap Database

The functional characterization of the connectivity-based parcellation-yielded subregions was based on behavioral domain and paradigm class meta data labels of the BrainMap database (cf. http://www.brainmap.org/taxonomy) using forward and reverse inferences (Eickhoff et al. 2011; Cieslik et al. 2013; Clos et al. 2013; Fox et al. 2014). Forward inference indicates the probability of observing activity in a brain region given knowledge of the psychological process, whereas reverse inference is the probability of a psychological process being present given information about activation in a particular brain region. For the forward inference approach, a subregion's functional profile

was determined by identifying the taxonomic labels for which the probability of finding activation in a specific subregion was significantly higher than the overall chance (across the entire database) of finding activation in that particular subregion as established using a binomial test ($P < 0.05$ corrected). For the reverse inference, a subregion's functional profile was determined by identifying the most likely behavioral domains and paradigm classes given activation in this subregion using Bayes' rule. Significance ($P < 0.05$ corrected) was assessed by means of a χ^2 test.

Results

Parcellation Scheme of the Human Brain in the Brainnetome Atlas

On the basis of the connectivity architecture derived from probabilistic tractography using in vivo dMRI data, we subdivided the brain into a total of 210 cortical areas and 36 subcortical regions based on the reproducibility of the parcellation between the subjects, characterized using Cramer's V, and the interhemispheric consistency of topological relationships between clusters, characterized by the topographic distance (TpD).

Given that the anatomical connectivity maps of each identified subregion at whole-brain level were generated, we used the remaining 245 subregions as seed targets to construct a 246×246 connectivity matrix in which each item represents the structural connectivity of all subregions, and each row represents the fingerprint of a subregion. To supplement the validity of topological distance (TpD), here, we compared the similarity of connectivity fingerprint of each putative pair across the 2 hemispheres. Given a specified ROI, a $K \times K$ matrix was derived from the connectivity matrix of each subject. In this matrix, K denotes the label number of subregions, row and column represent the label number of subregions in ascending order in the left and right hemisphere, respectively, and each entry represents the similarity (1 – cosine distance) between the fingerprints of 2 subregions in this ROI (see details in Supplementary Figs 2–7). From the nomenclature relating label number and the corresponding name, we can conclude that TpD is an effective index that is able to find the contralateral part with the most similar connectivity profile of a subregion. For the final atlas, the MPM including all of these subregions was created in a standard MNI space (Fig. 2; see Supplementary Fig. 1). The details of the parcellation results for each initial region (and the repeatability validation results using an independent dataset) are listed in Supplementary Figures 2–7.

One of the challenges that arise in the context of new brain parcellation schemes is the naming of the ensuing subregions in the Brainnetome Atlas. To denominate the identified subregions at the Brainnetome Atlas, we hence employed 2 kinds of nomenclature (cf. Supplementary Table 1). In particular, we followed the primary strategy of using the DK atlas labels providing the initial macroanatomic parcellation, followed by a numeric labeling of the clusters. While preferable for not implicating potentially unwarranted correspondence with previous (microstructural) brain maps, this solution has the disadvantage of being rather hard to follow. Acknowledging that most researchers will be more familiar with labeling schemes (broadly) based on the Brodmann atlas, we thus provide tentative labels following this nomenclature, incorporating more recent refinements where available (Vogt et al. 1995; Petrides and Pandya 1999, 2002; Ongur et al. 2003; Caspers et al. 2008; Scheperjans et al. 2008; Amunts et al. 2010; Morel et al. 2013). To facilitate using the current atlas and comparing it with other atlases, we have taken our parcellation results into careful consideration for maximum consistency with existing cyto-, myelo-, or receptor-based architectonic parcellations as follows. The naming of subregions in frontal lobe is similar to that of Ongur et al. (2003), Petrides and Pandya (1999), Petrides and Pandya (2002), and Amunts et al. (2010). The naming of subregions in insular lobe is similar to that of Morel et al. (2013). The naming of subregions in parietal lobe is similar to that of Caspers et al. (2008) and Scheperjans et al. (2008). The naming of subregions in cingulate gyrus is similar to that of Vogt et al. (1995). The naming of subregions in temporal lobe is similar to that of Brodmann's descriptions. Because of the mismatch with the existing architectonic maps, we have kept the macroanatomical descriptions to name the subregions in occipital lobe.

Taking the parcellation results from the right middle frontal gyrus (MFG) and right insular cortex as an example, we identified 7 subregions in the right MFG and 6 subregions in the right insula based on the assessment of split-half reliability (Cramer's V shown in Figs 3*B* and 4*B*). MPMs for the ensuing subregions (Figs 3*A* and 4*A*) across the 40 subjects indicate the topography of the defined subregions. The MFG was found to contain MFG-1(dorsal division of area 9/46), MFG-2 (inferior frontal junction, *IFJ*), MFG-3 (area 46), MFG-4 (ventral division of area 9/46), MFG-5 (ventrolateral area 8, A8*vl*), MFG-6 (ventrolateral area 6, A6*vl*), and MFG-7 (lateral area, 10l). The insular cortex was composed of INS-1 (the hypergranular insula, *G*), INS-2 (ventral agranular insula, *vIa*), INS-3 (dorsal agranular insula, *dIa*), INS-4 (ventral dysgranular and granular insula, *vId/vIg*), INS-5 (dorsal granular insula, *dIg*), and INS-6 (dorsal dysgranular insula, *dId*). In addition, the probability distribution for each subregion of the MFG and insula was calculated to characterize the individual variance (Figs 3*C* and 4*C*).

Anatomical and Functional Connectivity Patterns in the Brainnetome Atlas

To reveal the connectivity patterns of the identified subregions in detail, we first delineated the major fiber bundles connecting the respective subregion with the rest of the brain using the whole-brain probabilistic fiber tractography (Figs 3*D* and 4*D*). All anatomical connectivity maps will be released with the Brainnetome Atlas Viewer (Fig. 6*C*4,7) and presented on the interactive website (Fig. 6*B*2). Second, we obtained a connectivity matrix representing the structural connectivity between all identified subregions as shown in Figure 5A,*B* for intrahemispheric and Figure 5*C* for interhemispheric connections. The anatomical and functional connectivity maps as well as the detailed connectogram for each brain subregion are shown on the website (http://atlas.brainnetome.org; Fig. 6*B*2,4). Taking the right MFG-5, that is, area 8*vl*, as an example, we found that this area showed connections with the major frontal subregions (including areas 44*v*, 45*c*, inferior frontal sulcus (IFS), 6*vl*, 8*vl*, 9/46*d*, 9*m*, 6*m*, 6*dl*, 9l, 8*m*, and 8*dl*), the limbic area 24*rv*, the parietal subregions (including areas 7*pc*, 39*rv*, and 40*rd*), and the subcortical connections with the thalamus and basal ganglia subregions (Fig. 5*D*).

Furthermore, we acquired whole-brain rfMRI connectivity maps for all the subregions in the Brainnetome Atlas. The functional connectivity maps are shared online (Fig. 6*B*2) and will be released for use with the Brainnetome Atlas Viewer (Fig. 6*C*5,8). For example, Figs 3*D* and 4*D* illustrate the functional connectivity maps of the right MFG subregion (MFG-5, A8*vl*) and the right insular subregion (INS-3, *dIa*).

Mapping the Region-to-Tasks Associations of the Brainnetome Atlas

The functional characterizations of each subregion in the Brainnetome Atlas are illustrated based on their behavioral domain

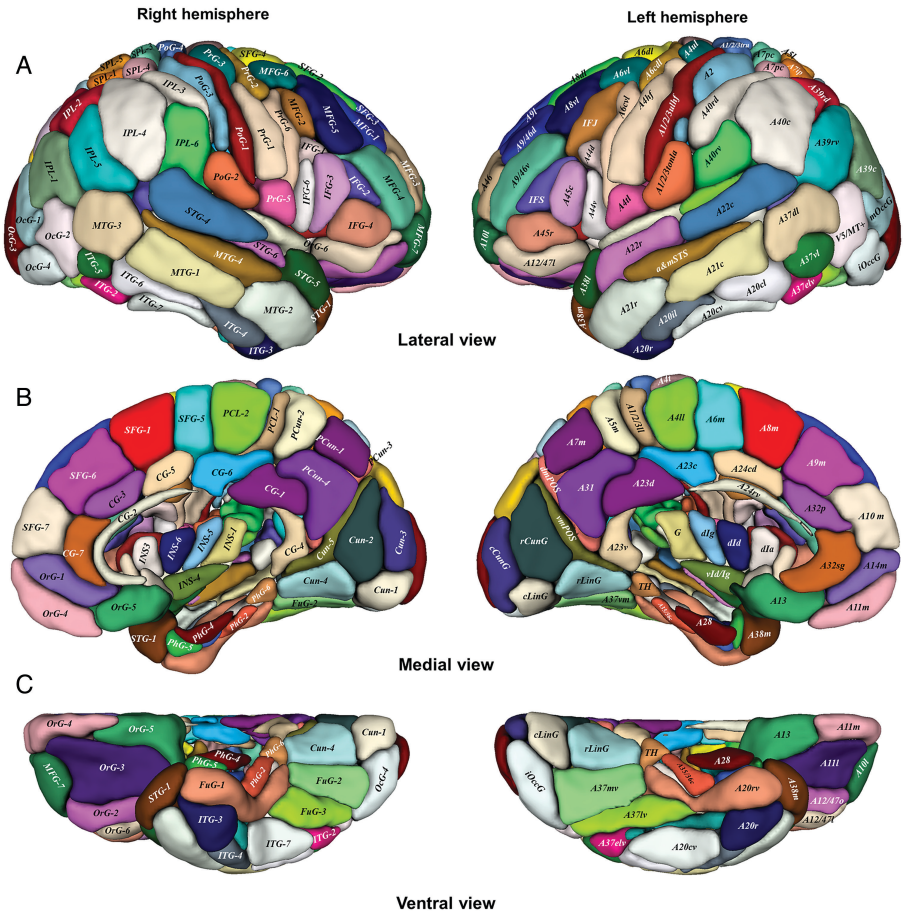

Figure 2. Parcellation scheme of the human brain in the Brainnetome Atlas. The MPM for each of the cortical subregions was created in standard MNI space ((*A*) lateral view, (*B*) medial view, (*C*) ventral view) and visualized using ITK-SNAP (www.itksnap.org). The atlas primarily combines ontological and nomenclature information from 2 sources, that is, anatomical and modified cytoarchitectonic descriptions. For convenience, these 2 types of descriptions are separately displayed in the left and right hemispheres. The details of the parcellation results for each subregion are listed in Table 1, and the online version is available at http://atlas.brainnetome.org/bnatlas.php. See also Supplementary Figures 1–5.

and paradigm class meta data labels following the BrainMap taxonomy (http://www.brainmap.org/taxonomy). For the 2 macroanatomic brain regions used to illustrate the Brainnetome Atlas process (MFG and INS, cf. above), the functional characterization of one of the ensuing subregions is shown in Figures 3*D* and 4*D*, respectively. It showed that A8*vl* was significantly associated with cognitive, for example, reasoning, explicit memory, working memory, and action-related processes, such as inhibition. In terms of paradigm classes, this area was significantly associated with flanker tasks, *n*-back tasks, and cued explicit recognition. The *dIa* was involved in perception, for example, pain somesthesis, action, such as inhibition, and cognition. This insular subregion was observed to be significantly activated by paradigms associated with pain monitoring/discrimination, reward tasks, and Sternberg tasks. The functional characterization for all Brainnetome Atlas subregions will again be available through the atlas viewer on our website.

Automatic Tractography-Based Parcellation Pipeline

As part of this work, we developed an integrated "Automatic Tractography-based Parcellation Pipeline (ATPP)" to realize the parcellation using automatic processing and massive parallel computing (Fig. 6A) that we share with the atlas. ATPP is a platform that combines tractography using FMRIB's diffusion toolbox with in-house MATLAB scripts for parcellation. It uses Oracle Grid Engine and MATLAB's Parallel Computing Toolbox for parallel computing across and within machines. Both a command line version and a graphical user interface (GUI) version are available. The GUI version is single-ROI oriented and therefore a user friendly method that allows the targeted analysis of any brain region defined, for example, by functional or structural findings (Cieslik et al. 2013; Muhle-Karbe et al. 2015). That is, while the Brainnetome Atlas provides a whole-brain parcellation at a (necessarily) coarser level, the distribution of the ATPP will allow researchers to use the same framework to address specific questions on local brain organization.

Interactive Website Viewer

The Brainnetome Atlas website, available at http://atlas.brainnetome.org, allows to fully explore the atlas and the various information associated with each subregion (Fig. 6B). To improve user interaction, the following functionalities were included: 1)

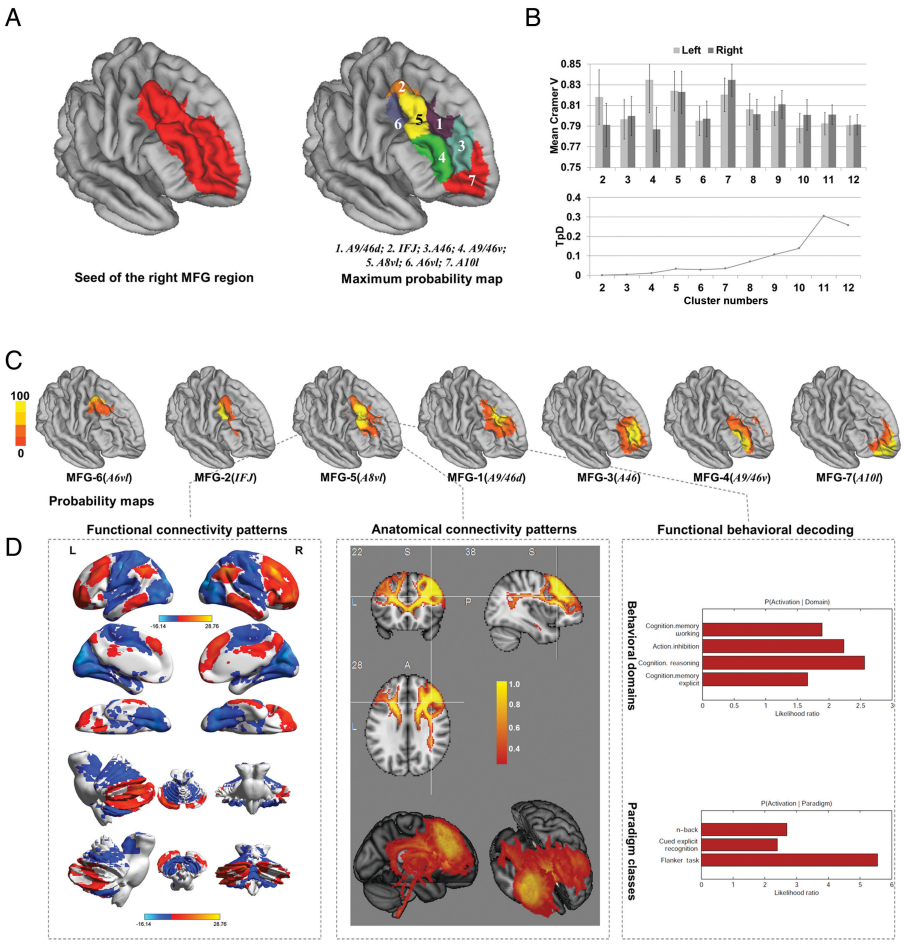

Figure 3. Brainnetome Atlas of the right middle frontal gyrus. (*A*) The right MFG ROI (on the left) and the MPM of the 7 subregions using a connectivity-based parcellation (on the right). We identified area 10l, area 46, dorsal and ventral divisions of area 9/46, area 6vl, area 8vl, and the IFJ subregion in the MFG. (*B*) The mean Cramer's V for each cluster number from 2 to 12. Cramer's V shows that 7 was the most stable solution for the right MFG. The TpD showed the similarity of the 7 solution for the topological arrangement between the 2 hemispheres. (*C*) The population probability maps for each MFG subregion. (*D*) Using the MFG-5, that is, A8vl, as an example: This figure shows the resting-state functional connectivity patterns (left), the tractographic signatures of the A8vl (middle), and the functional behavioral decoding (right).

Clicking a structure name in the tree will reveal that subregion in the slice viewer. At the same time, the behavioral domain and paradigm class analysis results, together with the anatomical and functional connectivity patterns, are updated in the atlas viewer. 2) Structural and functional connectivity maps are displayed with the possibility of full angle rotation. 3) By picking a bar that indicates another structure in the connectogram viewer, the user can navigate the connected structure and visualize the related information in the atlas viewer. 4) Users can search for a structure of interest. All branches with related keywords are highlighted so that the user can click to visualize the node.

StandAlone Brainnetome Atlas Viewer

We likewise provide a standalone Brainnetome Atlas Viewer running under MATLAB with a user friendly GUI (Fig. 6C), featuring subregion selection, template/surface selection, and connectivity visualization. The entire Brainnetome Atlas can be viewed as a maximum probabilistic map in a triplanar view. Navigation through the Brainnetome Atlas can be synchronized with a collection of widely used canonical templates/atlases. Once a subregion is selected, various information about this structure are displayed. Publications related to the selected subregion, if any, can be visited on PubMed. Subregions can be viewed as a 2D overlay of the MPM representation or the probabilistic map on the selected structural template and a 3D patch can be rendered on the cortical surface. Probably the key feature, however, is the possibility to generate ROI mask for further analyses by selecting atlas structures and probability thresholds.

Discussion

Capitalizing on the high resolution imaging data provided by the Human Connectome Project (Van Essen et al. 2013) and following the fundamental concept that long-range connectivity should represent 1 crucial determinant of regional specialization (Felleman and Van Essen 1991; Passingham et al. 2002; Jbabdi et al. 2015), we here present the Brainnetome Atlas representing of a connectivity-based parcellation of the brain into 246 subregions. Importantly, these subregions are extensively

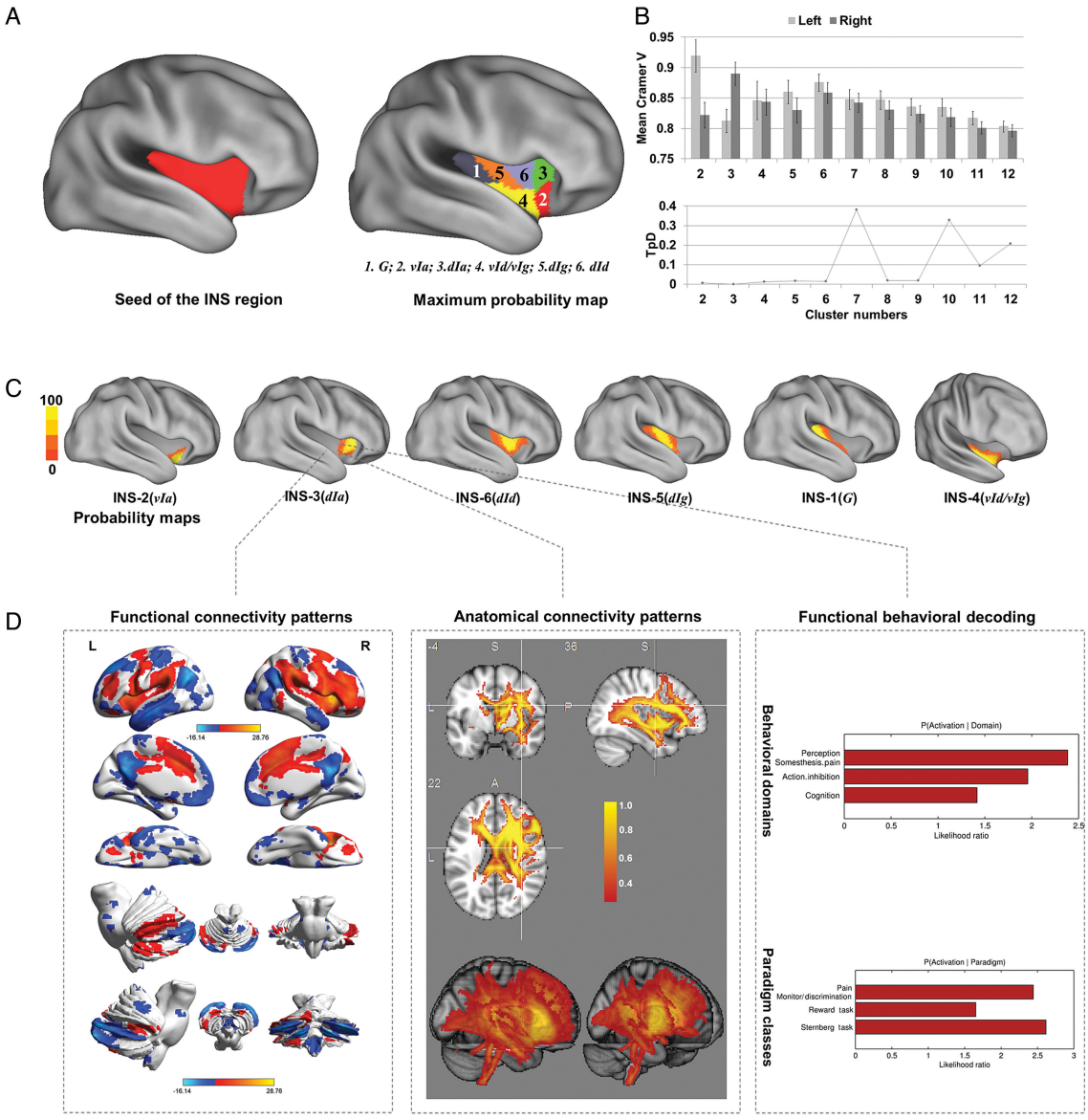

Figure 4. Brainnetome Atlas of the right insular cortex. (A) The right INS ROI (on the left) and the MPM of the 6 subregions using connectivity-based parcellation (on the right). Six subregions were identified in the insular cortex, including areas *G*, *vIa*, *dIa*, *vId/vIg*, *dIg*, and *dId*. (*B*) Cramer's V indicated that 6 was a local peak compared with the nearby solutions for the right INS. The TpD showed the similarity of the 6 solution for the topological arrangement between the 2 hemispheres. (*C*) The population probability maps for each INS subregion. (*D*) Using the INS-3, that is, area *dId*, as an example, this figure shows the resting-state functional connectivity patterns (left), the tractographic signatures of the area *dId* (middle), and the functional behavioral decoding (right).

characterized in terms of their structural and functional connectivity patterns as well as the associated functions as revealed by task-based neuroimaging. The Brainnetome Atlas thus provides a new framework for human brain research and in particular connectome analysis that overcomes several drawbacks of previous parcellation schemes: 1) it establishes a priori, biologically valid brain parcellation scheme of the entire cortical and subcortical gray matter into subregions showing a coherent pattern of anatomical connections, 2) it provides detailed characterizations of the structural and functional connectivity patterns for these, and 3) it decodes brain functions by establishing those tasks and contrasts that activated the respective area above chance in previous task-based functional neuroimaging studies.

Brainnetome Atlas: Towards a Framework for Multimodal Information Integration

Because of the variety of needs of different fields within neuroscience and the shortcomings of existing brain atlases, a new human brain atlas with a framework for integrating multimodal information is urgently needed (Evans et al. 2012; Amunts et al. 2014). Consequently, many studies have used different MRI modalities to identify individual brain region or provide more comprehensive maps of the cerebral cortex (Tzourio-Mazoyer et al. 2002; Desikan et al. 2006; Cohen, Fair, et al. 2008; Cohen, Lombardo, et al. 2008; Eickhoff et al. 2011; Wang et al. 2012; Fan et al. 2014; Wig et al. 2014; Laumann Timothy et al. 2015;

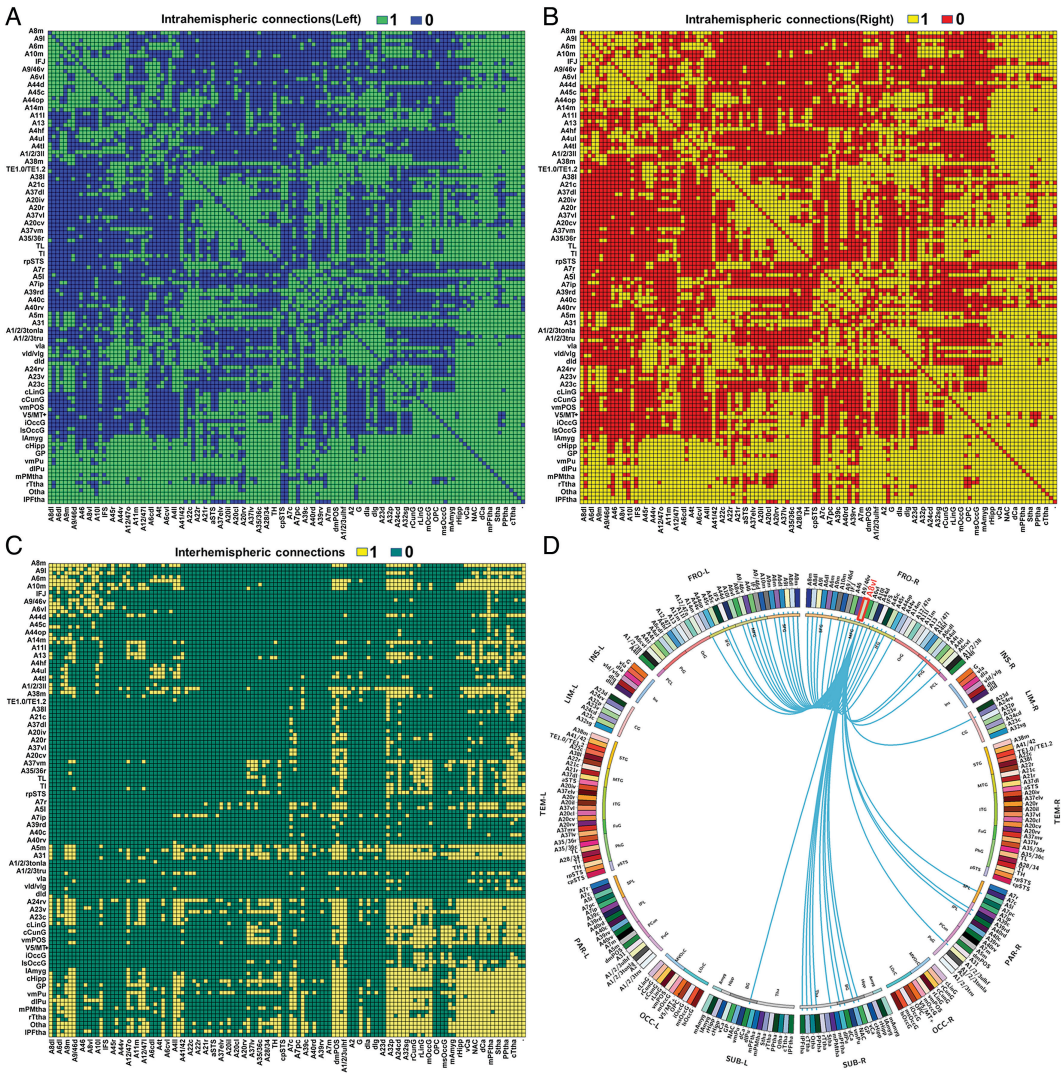

Figure 5. Connection matrices and connectogram of the Brainnetome Atlas. (*A*) The intrahemispheric connection matrix of the left hemisphere. (*B*) The intrahemispheric connection matrix of the right hemisphere. (*C*) The interhemispheric connection matrix across the 2 hemispheres. (*D*) Examples of the subregional connectograms for areas of the right MFG-5, that is, A8*vl*. The connectograms are represented using the Circos data visualization tool, with the left half depicting the left hemisphere and the right half depicting the right hemisphere. The hemispheres are divided into the frontal lobe, insular cortex, limbic lobe, temporal lobe, parietal lobe, occipital lobe, and subcortical structures.

Liu et al. 2015; Yang et al. 2015). While acknowledging that there is no consensus on which modality or aspect of brain organization may be most reflective of the brains' "true" organization (and in fact, there may be no single answer to this question), brain atlases are crucial to advance understanding of the human brain given that macroanatomical landmarks or coordinate systems are not valid indicators of regional specialization (Brett et al. 2002; Bohland et al. 2009; Evans et al. 2012). The Brainnetome Atlas addresses this need by providing a whole-brain parcellation of the human brain into distinct subregions based on the local structural connectivity architecture, that is, by identifying subregions that are maximally different from each other and maximally homogeneous internally in terms of their white matter connections. It thus provides an objective and stable starting point from which to explore the complex relationships between structure, connectivity, and function featuring the following advantages.

1. Robust and biologically plausible anatomical parcels: An increasing number of in vivo neuroimaging studies have demonstrated that fine-grained parcellations of large regions of the human brain are needed. The Brainnetome Atlas not only confirmed several differentiations from earlier cytoarchitectonic maps but also revealed numerous anatomical subdivisions that were not previously described (Liu et al. 2013; Fan et al. 2014). For example, in the atlas, the insular cortex has been subdivided into 6 subregions (Fig. 2; see Supplementary Fig. 5A). Although the correct parcellation of the human insular cortex has been disputed (Cauda and Vercelli 2013), the current parcellation, showing the highest split-half reliability of all cluster solutions, relates well to previous functional and histological maps of the insular cortex (Kurth, Eickhoff, et al. 2010; Kurth, Zilles, et al. 2010; Kelly et al. 2012; Chang et al. 2013; Morel et al. 2013), identifying a dorsal and ventral aspect of the anterior insula, a central

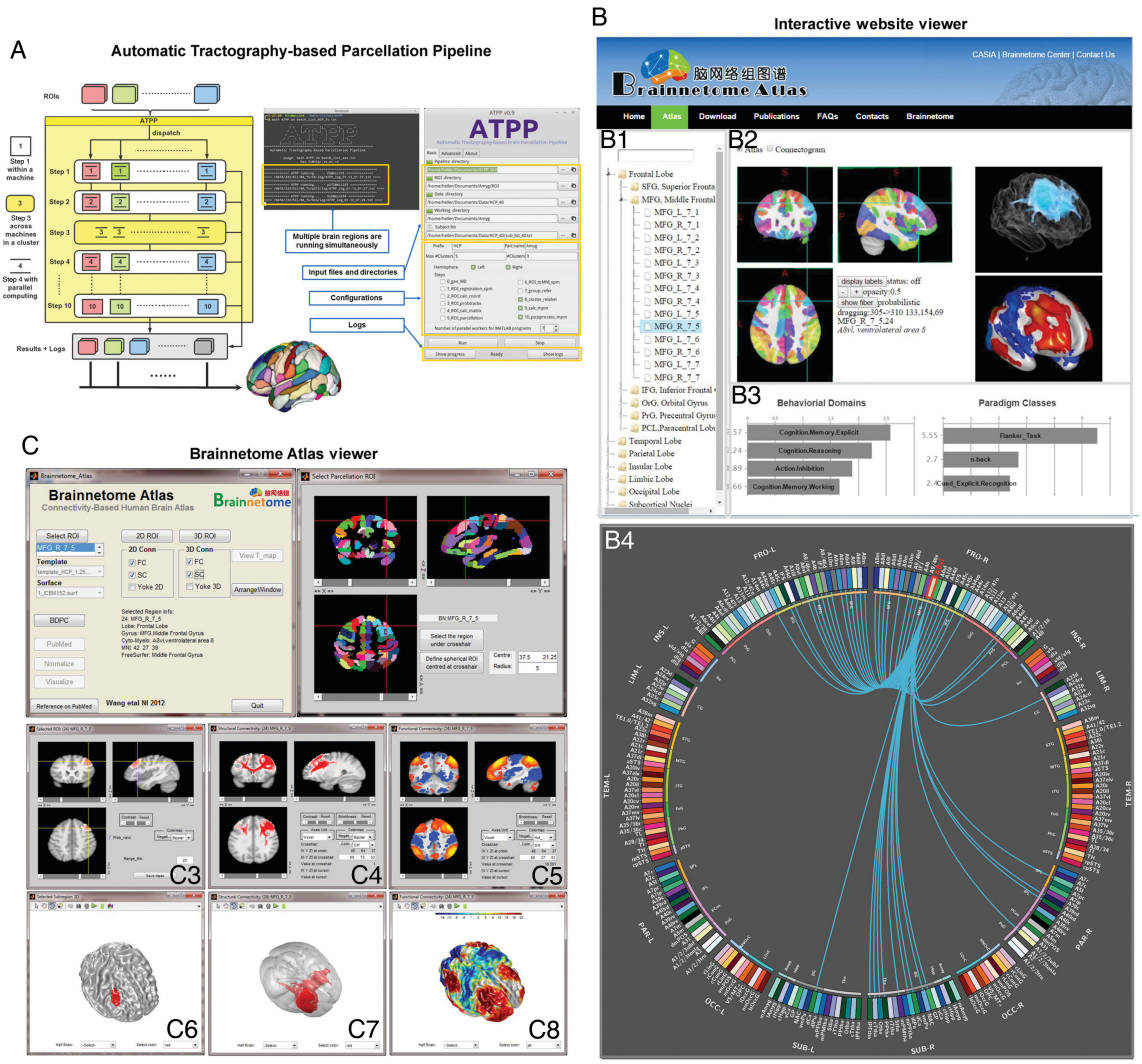

Figure 6. Resources of the Brainnetome Atlas: pipeline, Brainnetome Atlas Viewer, and interactive website. (*A*) Automatic Tractography-based Parcellation Pipeline (ATPP): The GUI version is single-ROI oriented; thus, it is a user friendly method that can modify some parameters to parcellate a specific brain region. The command line version is multi-ROI oriented, which can be used to parcellate many brain regions simultaneously. (*B*) The Brainnetome Atlas interactive website: The website makes all the information in the Brainnetome Atlas available to researchers. It provides a hierarchical tree of brain structures in the left panel (*B1*). The right panel contains an atlas viewer (*B2* and *B3*) that shows slice views together with a connectogram viewer (*B4*). (*C*) The Brainnetome Atlas Viewer (V1.0): The main window of the software contains push buttons, pull-down lists, and checkboxes for different function modules (*C1*), such as subregion selection, template/surface selection, and connectivity visualization. The entire Brainnetome Atlas contains 246 subregions and can be viewed as a maximum probabilistic map in a tri-planar view (*C2*). The subregion can be viewed as a 2D overlay on the selected structural template (*C3*) and a 3D patch can be rendered on the cortical surface (*C6*). Using the checkboxes, the structural and functional connectivities of the selected subregion can be viewed in both 2D tri-planar views (*C4* and *C5*) and 3D renderings (*C7* and *C8*) as probabilistic maps.

cluster, a more ventral component, and (2) posterior subregions. As another example, the inferior frontal gyrus contains 6 subregions that were robustly identified across subjects: the dorsal/ventral portions of area 44, the rostral and caudal subdivisions of area 45, the inferior fontal sulcus, and 1 cluster on the frontal operculum, which correspond to a combination of areas op8 and op9 (Fig. 2; see Supplementary Fig. 2C). This parcellation compares well with a parcellation scheme that was proposed based on the differential distribution of transmitter receptors (Amunts et al. 2010) and the differential inclusion in task activation networks (Clos et al. 2013).

2. Detailed description of anatomical and functional connections: One of the major drawbacks of several previous atlases is that they present rather isolated information, that is, are only reflective or brain organization from a single perspective. The Brainnetome Atlas in turn has been designed to enrich our understanding of human brain organization from a multimodal perspective. Combining diffusion MRI with tractography could allow reconstruction of the major fiber bundles, while functional connectivity analyses of BOLD functional MRI data could also provide a noninvasive way to assess in vivo the large-scale connectivity of the human brain. These approaches should enable researchers to identify connectivity patterns and relate this information to the parcellations in the Brainnetome Atlas. This should be useful in detailed investigations of particular subsystems.

Table 1 Ontology and nomenclature of brain areas and their abbreviations in the Brainnetome Atlas

Lobe	Gyrus	Left and right hemispheres	Label ID.L	Label ID.R	Modified cyto-architectonic	lh.MNI (X,Y,Z)	rh.MNI (X, Y, Z)
Frontal lobe	SFG, Superior frontal gyrus	SFG_L(R)_7_1	1	2	A8m, medial area 8	−5 ,15, 54	7, 16, 54
		SFG_L(R)_7_2	3	4	A8dl, dorsolateral area 8	−18, 24, 53	22, 26, 51
		SFG_L(R)_7_3	5	6	A9l, lateral area 9	−11, 49, 40	13, 48, 40
		SFG_L(R)_7_4	7	8	A6dl, dorsolateral area 6	−18, −1, 65	20, 4, 64
		SFG_L(R)_7_5	9	10	A6m, medial area 6	−6, −5, 58	7, −4, 60
		SFG_L(R)_7_6	11	12	A9m, medial area 9	−5, 36, 38	6, 38, 35
		SFG_L(R)_7_7	13	14	A10m, medial area 10	−8, 56, 15	8, 58, 13
	MFG, Middle frontal gyrus	MFG_L(R)_7_1	15	16	A9/46d, dorsal area 9/46	−27, 43, 31	30, 37, 36
		MFG_L(R)_7_2	17	18	IFJ, inferior frontal junction	−42, 13, 36	42, 11, 39
		MFG_L(R)_7_3	19	20	A46, area 46	−28, 56, 12	28, 55, 17
		MFG_L(R)_7_4	21	22	A9/46v, ventral area 9/46	−41, 41, 16	42, 44, 14
		MFG_L(R)_7_5	23	24	A8vl, ventrolateral area 8	−33, 23, 45	42, 27, 39
		MFG_L(R)_7_6	25	26	A6vl, ventrolateral area 6	−32, 4, 55	34, 8, 54
		MFG_L(R)_7_7	27	28	A10l, lateral area 10	−26, 60, −6	25, 61, −4
	IFG, Inferior frontal gyrus	IFG_L(R)_6_1	29	30	A44d, dorsal area 44	−46, 13, 24	45, 16, 25
		IFG_L(R)_6_2	31	32	IFS, inferior frontal sulcus	−47, 32, 14	48, 35, 13
		IFG_L(R)_6_3	33	34	A45c, caudal area 45	−53, 23, 11	54, 24, 12
		IFG_L(R)_6_4	35	36	A45r, rostral area 45	−49, 36, −3	51, 36, −1
		IFG_L(R)_6_5	37	38	A44op, opercular area 44	−39, 23, 4	42, 22, 3
		IFG_L(R)_6_6	39	40	A44v, ventral area 44	−52, 13, 6	54, 14, 11
	OrG, Orbital gyrus	OrG_L(R)_6_1	41	42	A14m, medial area 14	−7, 54, −7	6, 47, −7
		OrG_L(R)_6_2	43	44	A12/47o, orbital area 12/47	−36, 33, −16	40, 39, −14
		OrG_L(R)_6_3	45	46	A11l, lateral area 11	−23, 38, −18	23, 36, −18
		OrG_L(R)_6_4	47	48	A11m, medial area 11	−6, 52, −19	6, 57, −16
		OrG_L(R)_6_5	49	50	A13, area 13	−10, 18, −19	9, 20, −19
		OrG_L(R)_6_6	51	52	A12/47l, lateral area 12/47	−41, 32, −9	42, 31, −9
	PrG, Precentral gyrus	PrG_L(R)_6_1	53	54	A4hf, area 4(head and face region)	−49, −8, 39	55, −2, 33
		PrG_L(R)_6_2	55	56	A6cdl, caudal dorsolateral area 6	−32, −9, 58	33, −7, 57
		PrG_L(R)_6_3	57	58	A4ul, area 4(upper limb region)	−26, −25, 63	34, −19, 59
		PrG_L(R)_6_4	59	60	A4t, area 4(trunk region)	−13, −20, 73	15, −22, 71
		PrG_L(R)_6_5	61	62	A4tl, area 4(tongue and larynx region)	−52, 0, 8	54, 4, 9
		PrG_L(R)_6_6	63	64	A6cvl, caudal ventrolateral area 6	−49, 5, 30	51, 7, 30
	PCL, Paracentral lobule	PCL_L(R)_2_1	65	66	A1/2/3ll, area 1/2/3 (lower limb region)	−8, −38, 58	10, −34, 54
		PCL_L(R)_2_2	67	68	A4ll, area 4, (lower limb region)	−4, −23, 61	5, −21, 61

Continued

Table 1 Continued

Lobe	Gyrus	Left and right hemispheres	Label ID.L	Label ID.R	Modified cyto-architectonic	lh.MNI (X,Y,Z)	rh.MNI (X, Y, Z)
Temporal lobe	STG, Superior temporal gyrus	STG_L(R)_6_1	69	70	A38m, medial area 38	−32, 14, −34	31, 15, −34
		STG_L(R)_6_2	71	72	A41/42, area 41/42	−54, −32, 12	54, −24, 11
		STG_L(R)_6_3	73	74	TE1.0 and TE1.2	−50, −11, 1	51, −4, −1
		STG_L(R)_6_4	75	76	A22c, caudal area 22	−62, −33, 7	66, −20, 6
		STG_L(R)_6_5	77	78	A38l, lateral area 38	−45, 11, −20	47, 12, −20
		STG_L(R)_6_6	79	80	A22r, rostral area 22	−55, −3, −10	56, −12, −5
	MTG, Middle temporal gyrus	MTG_L(R)_4_1	81	82	A21c, caudal area 21	−65, −30, −12	65, −29, −13
		MTG_L(R)_4_2	83	84	A21r, rostral area 21	−53, 2, −30	51, 6, −32
		MTG_L(R)_4_3	85	86	A37dl, dorsolateral area 37	−59, −58, 4	60, −53, 3
		MTG_L(R)_4_4	87	88	aSTS, anterior superior temporal sulcus	−58, −20, −9	58, −16, −10
	ITG, Inferior temporal gyrus	ITG_L(R)_7_1	89	90	A20iv, intermediate ventral area 20	−45, −26, −27	46, −14, −33
		ITG_L(R)_7_2	91	92	A37elv, extreme lateroventral area 37	−51, −57, −15	53, −52, −18
		ITG_L(R)_7_3	93	94	A20r, rostral area 20	−43, −2, −41	40, 0, −43
		ITG_L(R)_7_4	95	96	A20il, intermediate lateral area 20	−56, −16, −28	55, −11, −32
		ITG_L(R)_7_5	97	98	A37vl, ventrolateral area 37	−55, −60, −6	54, −57, −8
		ITG_L(R)_7_6	99	100	A20cl, caudolateral of area 20	−59, −42, −16	61, −40, −17
		ITG_L(R)_7_7	101	102	A20cv, caudoventral of area 20	−55, −31, −27	54, −31, −26
	FuG, Fusiform gyrus	FuG_L(R)_3_1	103	104	A20rv, rostroventral area 20	−33, −16, −32	33, −15, −34
		FuG_L(R)_3_2	105	106	A37mv, medioventral area 37	−31, −64, −14	31, −62, −14
		FuG_L(R)_3_3	107	108	A37lv, lateroventral area 37	−42, −51, −17	43, −49, −19
	PhG, Parahippocampal gyrus	PhG_L(R)_6_1	109	110	A35/36r, rostral area 35/36	−27, −7, −34	28, −8, −33
		PhG_L(R)_6_2	111	112	A35/36c, caudal area 35/36	−25, −25, −26	26, −23, −27
		PhG_L(R)_6_3	113	114	TL, area TL (lateral PPHC, posterior parahippocampal gyrus)	−28, −32, −18	30, −30, −18
		PhG_L(R)_6_4	115	116	A28/34, area 28/34 (EC, entorhinal cortex)	−19, −12, −30	19, −10, −30
		PhG_L(R)_6_5	117	118	TI, area TI(temporal agranular insular cortex)	−23, 2, −32	22, 1, −36
		PhG_L(R)_6_6	119	120	TH, area TH (medial PPHC)	−17, −39, −10	19, −36, −11
	pSTS, Posterior superior temporal sulcus	pSTS_L(R)_2_1	121	122	rpSTS, rostroposterior superior temporal sulcus	−54, −40, 4	53, −37, 3
		pSTS_L(R)_2_2	123	124	cpSTS, caudoposterior superior temporal sulcus	−52, −50, 11	57, −40, 12

Parietal lobe	SPL, Superior parietal lobule	SPL_L(R)_5_1	125	126	A7r, rostral area 7	−16, −60, 63	19, −57, 65
		SPL_L(R)_5_2	127	128	A7c, caudal area 7	−15, −71, 52	19, −69, 54
		SPL_L(R)_5_3	129	130	A5l, lateral area 5	−33, −47, 50	35, −42, 54
		SPL_L(R)_5_4	131	132	A7pc, postcentral area 7	−22, −47, 65	23, −43, 67
		SPL_L(R)_5_5	133	134	A7ip, intraparietal area 7(hIP3)	−27, −59, 54	31, −54, 53
	IPL, Inferior parietal lobule	IPL_L(R)_6_1	135	136	A39c, caudal area 39(PGp)	−34, −80, 29	45, −71, 20
		IPL_L(R)_6_2	137	138	A39rd, rostrodorsal area 39(Hip3)	−38, −61, 46	39, −65, 44
		IPL_L(R)_6_3	139	140	A40rd, rostrodorsal area 40(PFt)	−51, −33, 42	47, −35, 45
		IPL_L(R)_6_4	141	142	A40c, caudal area 40(PFm)	−56, −49, 38	57, −44, 38
		IPL_L(R)_6_5	143	144	A39rv, rostroventral area 39(PGa)	−47, −65, 26	53, −54, 25
		IPL_L(R)_6_6	145	146	A40rv, rostroventral area 40(PFop)	−53, −31, 23	55, −26, 26
	Pcun, Precuneus	PCun_L(R)_4_1	147	148	A7m, medial area 7(PEp)	−5, −63, 51	6, −65, 51
		PCun_L(R)_4_2	149	150	A5m, medial area 5(PEm)	−8, −47, 57	7, −47, 58
		PCun_L(R)_4_3	151	152	dmPOS, dorsomedial parietooccipital sulcus(PEr)	−12, −67, 25	16, −64, 25
		PCun_L(R)_4_4	153	154	A31, area 31 (Lc1)	−6, −55, 34	6, −54, 35
	PoG, Postcentral gyrus	PoG_L(R)_4_1	155	156	A1/2/3ulhf, area 1/2/3(upper limb, head and face region)	−50, −16, 43	50, −14, 44
		PoG_L(R)_4_2	157	158	A1/2/3tonIa, area 1/2/3(tongue and larynx region)	−56, −14, 16	56, −10, 15
		PoG_L(R)_4_3	159	160	A2, area 2	−46, −30, 50	48, −24, 48
		PoG_L(R)_4_4	161	162	A1/2/3tru, area 1/2/3(trunk region)	−21, −35, 68	20, −33, 69
Insular lobe	INS, Insular gyrus	INS_L(R)_6_1	163	164	G, hypergranular insula	−36, −20, 10	37, −18, 8
		INS_L(R)_6_2	165	166	vIa, ventral agranular insula	−32, 14, −13	33, 14, −13
		INS_L(R)_6_3	167	168	dIa, dorsal agranular insula	−34, 18, 1	36, 18, 1
		INS_L(R)_6_4	169	170	vId/vIg, ventral dysgranular and granular insula	−38, −4, −9	39, −2, −9
		INS_L(R)_6_5	171	172	dIg, dorsal granular insula	−38, −8, 8	39, −7, 8
		INS_L(R)_6_6	173	174	dId, dorsal dysgranular insula	−38, 5, 5	38, 5, 5
Limbic lobe	CG, Cingulate gyrus	CG_L(R)_7_1	175	176	A23d, dorsal area 23	−4, −39, 31	4, −37, 32
		CG_L(R)_7_2	177	178	A24rv, rostroventral area 24	−3, 8, 25	5, 22, 12
		CG_L(R)_7_3	179	180	A32p, pregenual area 32	−6, 34, 21	5, 28, 27
		CG_L(R)_7_4	181	182	A23v, ventral area 23	−8, −47, 10	9, −44, 11
		CG_L(R)_7_5	183	184	A24cd, caudodorsal area 24	−5, 7, 37	4, 6, 38
		CG_L(R)_7_6	185	186	A23c, caudal area 24	−7, −23, 41	6, −20, 40
		CG_L(R)_7_7	187	188	A32sg, subgenual area 32	−4, 39, −2	5, 41, 6
Occipital lobe	MVOcC, MedioVentral occipital cortex	MVOcC _L(R)_5_1	189	190	cLinG, caudal lingual gyrus	−11, −82, −11	10, −85, −9
		MVOcC _L(R)_5_2	191	192	rCunG, rostral cuneus gyrus	−5, −81, 10	7, −76, 11
		MVOcC _L(R)_5_3	193	194	cCunG, caudal cuneus gyrus	−6, −94, 1	8, −90, 12
		MVOcC _L(R)_5_4	195	196	rLinG, rostral lingual gyrus	−17, −60, −6	18, −60, −7
		MVOcC _L(R)_5_5	197	198	vmPOS,ventromedial parietooccipital sulcus	−13, −68, 12	15, −63, 12
	LOcC, Lateral occipital cortex	LOcC_L(R)_4_1	199	200	mOccG, middle occipital gyrus	−31, −89, 11	34, −86, 11
		LOcC _L(R)_4_2	201	202	V5/MT+, area V5/MT+	−46, −74, 3	48, −70, −1
		LOcC _L(R)_4_3	203	204	OPC, occipital polar cortex	−18, −99, 2	22, −97, 4
		LOcC_L(R)_4_4	205	206	iOccG, inferior occipital gyrus	−30, −88, −12	32, −85, −12
		LOcC_L(R)_2_1	207	208	msOccG, medial superior occipital gyrus	−11, −88, 31	16, −85, 34
		LOcC_L(R)_2_2	209	210	lsOccG, lateral superior occipital gyrus	−22, −77, 36	29, −75, 36

Continued

Table 1 Continued

Lobe	Gyrus	Left and right hemispheres	Label ID.L	Label ID.R	Modified cyto-architectonic	lh.MNI (X,Y,Z)	rh.MNI (X, Y, Z)
Subcortical nuclei	Amyg, Amygdala	Amyg_L(R)_2_1	211	212	mAmyg, medial amygdala	−19, −2, −20	19, −2, −19
		Amyg_L(R)_2_2	213	214	lAmyg, lateral amygdala	−27, −4, −20	28, −3, −20
	Hipp, Hippocampus	Hipp_L(R)_2_1	215	216	rHipp, rostral hippocampus	−22, −14, −19	22, −12, −20
		Hipp_L(R)_2_2	217	218	cHipp, caudal hippocampus	−28, −30, −10	29, −27, −10
	BG, Basal ganglia	BG_L(R)_6_1	219	220	vCa, ventral caudate	−12, 14, 0	15, 14, −2
		BG_L(R)_6_2	221	222	GP, globus pallidus	−22, −2, 4	22, −2, 3
		BG_L(R)_6_3	223	224	NAC, nucleus accumbens	−17, 3, −9	15, 8, −9
		BG_L(R)_6_4	225	226	vmPu, ventromedial putamen	−23, 7, −4	22, 8, −1
		BG_L(R)_6_5	227	228	dCa, dorsal caudate	−14, 2, 16	14, 5, 14
		BG_L(R)_6_6	229	230	dlPu, dorsolateral putamen	−28, −5, 2	29, −3, 1
	Tha, Thalamus	Tha_L(R)_8_1	231	232	mPFtha, medial pre-frontal thalamus	−7, −12, 5	7, −11, 6
		Tha_L(R)_8_2	233	234	mPMtha, pre-motor thalamus	−18, −13, 3	12, −14, 1
		Tha_L(R)_8_3	235	236	Stha, sensory thalamus	−18, −23, 4	18, −22, 3
		Tha_L(R)_8_4	237	238	rTtha, rostral temporal thalamus	−7, −14, 7	3, −13, 5
		Tha_L(R)_8_5	239	240	PPtha, posterior parietal thalamus	−16, −24, 6	15, −25, 6
		Tha_L(R)_8_6	241	242	Otha, occipital thalamus	−15, −28, 4	13, −27, 8
		Tha_L(R)_8_7	243	244	cTtha, caudal temporal thalamus	−12, −22, 13	10, −14, 14
		Tha_L(R)_8_8	245	246	lPFtha, lateral pre-frontal thalamus	−11, −14, 2	13, −16, 7

3. Functional interpretation of the Brainnetome Atlas: One of the key challenges in human brain research is to reconcile the regional segregation of the cortex into distinct modules with the representation of mental functions as provided by task-based neuroimaging data. Because it was designed as a framework for a variety of resources, the Brainnetome Atlas is suitable for integrating a wealth of information from existing neuroimaging studies. In this study, we used BrainMap (Laird et al. 2009, 2011; Fox et al. 2014), currently the largest database of brain activation studies, to provide an initial assessment of the mental processes that may be sustained by each subregion of the Brainnetome Atlas. These descriptions, which are shared with the community, thus provide an objective guideline to the functional interpretations of any effects observed within a given Brainnetome Atlas subregion.
4. Data sharing: The Brainnetome Atlas can be flexibly wrapped into common reference spaces, such as the volumetric MNI space, the vertex-based FreeSurfer, or the Caret surface template. The atlas together with its related software is available for download to serve as a shared community resource (http://atlas.brainnetome.org, Fig. 6*B*). The pipeline software is open to the community to facilitate the parcellation of specific brain regions of interest (Fig. 6*A*). The Brainnetome Atlas Viewer was coded in MATLAB so that it can easily be implemented into commonly used brain MRI processing pipelines (Fig. 6*C*). In addition, the atlas will be useful for the definition of masks for seeding specific a priori cortical regions or networks of interest in prospective neuroimaging studies.

Relationship Between Connectivity Architecture and Microstructural Organization

Animal studies have indicated that connectivity architecture and microstructural organization are 2 complementary anatomical properties of the brain (Scannell et al. 1995; Barbas and Rempel-Clower 1997; Passingham et al. 2002; Hilgetag and Grant 2010). For example, by observing the laminar organization of areas in the monkey prefrontal cortex, Barbas and Rempel-Clower (1997) found that the cortical structure could predict the pattern and relative laminar distribution of cortico-cortical connections. Furthermore, it has been shown that cortico-cortical connectivity patterns exert strong effects on both the anatomical and functional characteristics of a specific brain region (Rempel-Clower and Barbas 2000; Glickfeld et al. 2013). Assessing the relationship between microstructure and connectivity is important to advance our understanding of brain organization, but a direct comparison between functional in vivo and anatomical postmortem studies is possible only in experimental animals. In turn, studies on the relationship between microstructure and function or connectivity in humans need to rely on across-subject analysis by means of probabilistic cytoarchitectonic maps in standard space (Eickhoff et al. 2005; Zilles and Amunts 2010). Such analyses have provided evidence for distinctions between (neighboring) histologically defined areas in terms of their structural and functional connectivity patterns (Eickhoff et al. 2010; Bludau et al. 2014; Palomero-Gallagher et al. 2015).

The importance of connectivity in determining functional specialization, however, suggests that parcellating brain regions based on their connectional architecture may provide important complementary information on human brain organization. For example, a recent study predicted which parts of the fusiform gyrus are involved in face recognition based on structural connectivity patterns (Saygin et al. 2012). In addition, it has been

shown that connectivity-based parcellation may closely follow histological subdivisions (Anwander et al. 2007; Klein et al. 2007) but also reveal additional subdivisions (Liu et al. 2013; Fan et al. 2014). The latter case is actually not particularly surprising, considering that intrinsic (cyto- or receptorarchitecture) and extrinsic (long-range connectivity) conjointly define the functional property of a given brain location (Eickhoff and Grefkes 2011). That is, it may be the intersection between microstructural and connectivity maps that defines specialization.

Closing the gap between these 2 approaches to parcellation still needs to be addressed. Specifically, additional work is needed to untangle the complex relationship between the brain's microstructural organization and its connectivity architecture as well as their roles in determining the brain's functional organization. In a recently published study (van den Heuvel et al. 2015), researchers performed a cross-scale examination and found that the organization of macroscale connectivity derived from diffusion MRI data correlates with cortical variation in cytoarchitectonics, in particular with the size of neurons in cortical layer 3. Other studies have also provided first experimental evidence that brain function arises from a combination of local infrastructure (microstructural/molecular features) and connectivity (Passingham et al. 2002; Scholtens et al. 2014; Barbas 2015). Therefore, combining connectivity-based parcellation results with probabilistic maps of microstructure could hold great promise for relating brain structure to function at the macroscopic scale.

Connectivity-Based Parcellation Using Multimodal Connectivity Information

Many approaches to parcellating the brain into subregions using different connectivity features have recently become available. These include tractography-based anatomical connectivity (Behrens et al. 2003; Johansen-Berg et al. 2004), resting-state functional connectivity (Cohen, Fair, et al. 2008; Cohen, Lombardo, et al. 2008; Nelson et al. 2010), structural covariance (Cohen, Fair, et al. 2008; Cohen, Lombardo, et al. 2008; Kelly et al. 2012), and meta-analysis-based functional coactivation (Eickhoff et al. 2011). However, the biological basis of these methods and what we can infer from these imaging modalities are not yet fully understood (Eickhoff et al. 2015). The current version of the Brainnetome Atlas was created using structural connectivity patterns as estimated by diffusion-weighted imaging and hence primarily relies on direct connections as opposed to indirect, multisynaptic interactions as revealed, for example, by resting-state or task-based functional connectivity. Several studies have focused on the relationship between anatomical and functional connectivity indicating that resting-state connectivity (Honey et al. 2009; van den Heuvel et al. 2009) and meta-analytic coactivations (Eickhoff et al. 2010) at least to some degree reflect the underlying anatomical connectivity architecture of the human brain. Finally, it has been shown that structural covariance patterns are largely in agreement with the aforementioned methods (Kelly et al. 2012). Although its biological significance remains controversial, it is hence assumed that functional connectivity should at least contribute to the patterns of structural covariance (Mechelli et al. 2005; Alexander-Bloch et al. 2013).

The other important aspect to consider in the construction of brain atlases, or more general, the definition of brain regions is the distinction between methods focused on either the clustering or the detection of borders. While similar in their final appearance, the former are driven by aggregating locations (voxels) with similar properties, whereas the later are aimed at identifying abrupt changes in the respective feature. The second relates to the nature of the features being either locally (such as cyto- or receptorarchitecture) or globally (such as connectivity profiles). To synthesize the existing brain parcellation studies, we may hence distinguish a "2 × 2" matrix of ways that have been used to generate brain atlases: regionally versus globally and by clustering or by border detection. The JuBrain cytoarchitectonic atlas and other histology-based atlases are examples of regional border detection (Brodmann 1909; Von Economo and Koskinas 1925; Zilles and Amunts 2010), while whole-brain parcellation studies based on rfMRI or dMRI may be realized by either global border detection (Wig et al. 2014; Gordon et al. 2016) or global clustering (Craddock et al. 2012; Moreno-Dominguez et al. 2014). In this framework, the Brainnetome Atlas would represent an example of clustering based on a global feature (connectivity).

Given the heterogeneity of both features and methods that may be used to parcellate the brain into distinct subregions, one of the particular challenges will be to examine the consistency or inconsistency of the ensuing parcellations and to evaluate different brain parcellation schemes. Using resting-state connectivity, meta-analytic coactivation and structural covariance, but not fiber tracking, Kelly et al. (2012) found a consistent pattern in the parcellations of the insula. In our recent work, we consistently identified 5 subregions in the superior parietal lobule of each hemisphere based on its anatomical connections as well as its resting-state connectivity and coactivation patterns (Yang et al. 2015). Further systematic comparison—across modalities, features, and methods—of the maps that may be computed using connectivity-based parcellation is still needed. Such integration would not only be crucial to obtain a more comprehensive picture of human brain organization, but in particular also to better understand the relationship between the different approaches and to arrive at a mechanistic relationship between the different aspects of brain organization (Amunts et al. 2014).

Methodological Considerations

The Brainnetome Atlas provides a cross-validated, robust group-level parcellation of the human brain, but ultimately individual, subject-level parcellations will be required to reflect interindividual variability in the location of brain modules (Barnes et al. 2011; Fonov et al. 2011; Laumann Timothy et al. 2015). In that context, we note that the parcellation current scheme is consistent with our previous parcellations of specific regions, including the frontal pole (Liu et al. 2013), temporal pole (Fan et al. 2014), parahippocampal region (Zhuo et al. 2016), and superior (Wang et al. 2015) and inferior parietal lobules (Wang et al. 2012) based on a different set of subjects. While reassuring, it still remains to be tested, how reliable individual brains may be parcellated using structural connectivity information and how the ensuing maps relate to other aspects of interindividual variability such as age and gender.

In forming the Brainnetome Atlas, we identified the following key issues for further consideration: 1) Development of reliable clustering algorithms and effective measures for validating the quality of parcellations needs to be further explored. Here, we used across-subject consistency as the key cluster-validity criterion, which is in line with previous work (Beckmann et al. 2009; Liu et al. 2013; Fan et al. 2014; Neubert et al. 2014), but may introduce a bias against more (spatially) variable patterns. 2) Maintaining the macroscopically visible sulcal and gyral anatomy so that we could provide an intuitive description of the location of the activations motivated by the use of the DK atlas as the initial parcellation. We have attempted to follow the widely accepted

anatomical conventions and then to further divide the brain regions into subregions using tractography-based parcellation. It should be acknowledged, however, that the DK atlas boundaries provide an a priori parcellation that may not be related to the actual differentiation of the cortex into distinct areas based on pure connectivity profiles. Additionally, the macroanatomy is generally a rather poor predictor of microstructural boundaries, and hence, further work may be warranted on the relationship between the Brainnetome Atlas and functional or microstructural parcellations at various scales. 3) To calculate the population-based probabilistic maps, it is vital to register the individual parcellation results to the commonly used MNI space. Recently, few groups have begun trying to work with the structural connectivity-based registration or fusing the connectivity information with the cortical anatomy (Gutman et al. 2014; Wang et al. 2014). However, such kind of registration methods based on structural connectivity is still very experimental and not well developed yet. The macro-anatomy-based registration is still the standard of the field, and we are keeping with the established approach in forming the Brainnetome Atlas. 4) The other important issue for this framework is the validation of the connectivity-based brain atlas (Klein et al. 2007; Gordon et al. 2016; Lefranc et al. 2016). The connectivity-based boundaries within the initial macroanatomical cortical areas are validated using another independent dataset with different scan parameters. The reproducible results from the independent dataset show good consistency with the parcellation results based on the HCP data.

Conclusions and Outlook

The long-term aim of the Brainnetome Project is to understand the organizing principles of the brain. The current version of the Brainnetome Atlas will facilitate investigations into structure–function relationships and holds promise for the identification of new biomarkers for diagnostic and clinical studies. In the future, however, novel methodologies and brain-mapping techniques should evolve and allow an enhanced assessment of the structure, function, and spatiotemporal changes in the human brain on different spatial and temporal scales. The Brainnetome Atlas should thus be regarded as a starting point, which will enable the generation of future brain atlases that are even more fine-grained and advance from single anatomical descriptions to an integrated atlas that includes structure, function, and connectivity, together with other potential sources of information (Amunts et al. 2014). The next stage of the Brainnetome Atlas will be multimodal instead of unimodal and dynamic instead of static by including information on spatiotemporal changes during normal development or aging as well as disease-related effects. Finally, integration with gene expression data should provide entirely novel insights into human brain organization. A recent study that analyzed brain imaging and gene expression data found that large-scale resting-state functional brain networks correlated with the expression of genes that code for ion channels and other synaptic functions (Richiardi et al. 2015). In a preliminary study of the relationship between genetics and brain parcellation, we noninvasively investigated the genetic influences on a fine-grained topological arrangement of the human cerebral cortex using MRI data from twins (Cui et al. 2015). While far from being understood and readily used, such genetic information will be crucial for the next-generation human brain atlas by linking phenotypically observed effects to genetic causes. While human brain atlasing is thus not only an endeavor that has been ongoing for more than a century but also one that will see constant changes and refinement, the current Brainnetome Atlas represents an important step in this development by providing the first whole-brain parcellation based on structural (connectivity) information on the basis of a robust cross-validation in a high-quality in vivo dataset.

Authors' Contributions

T.J. proposed the concept and designed the protocol. L.F., H.L., J.Z., J.W., and Y.Z. performed experiments and analyzed data. C.C., L. C., Z.Y., and S.X. developed the software and website. A.R.L., P.T. F., and S.B.E supplied the BrainMap database and further analyses tools. T.J., L.F., and C.Y. led the project and supervised experiments. All authors contributed to the writing of the manuscript.

Supplementary Material

Supplementary material can be found at: http://www.cercor.oxfordjournals.org/.

Funding

This work was partially supported by the National Key Basic Research and Development Program (973) (Grant No. 2011CB707801 and 2012CB720702), the Strategic Priority Research Program of the Chinese Academy of Sciences (Grant No. XDB02030300), the Natural Science Foundation of China (Grant Nos. 91432302, 91132301, 81501179, and 81270020), the Deutsche Forschungsgemeinschaft (DFG, EI 816/4-1; EI 816/6-1), the National Institute of Mental Health (R01-MH074457) and the Helmholtz Portfolio Theme "Supercomputing and Modeling for the Human Brain" and the European Union Seventh Framework Programme (FP7/2007-2013) under grant agreement no. 604102 (Human Brain Project), and Open Project Funding of National Key Laboratory of Cognitive Neuroscience and Learning-Beijing Normal University (Grant CNLYB1410).

Notes

Data were provided by the Human Connectome Project, WU-Minn Consortium (Principal Investigators: David Van Essen, and Kamil Ugurbil; 1U54MH091657) funded by the 16 NIH Institutes and Centers that support the NIH Blueprint for Neuroscience Research; and by the McDonnell Center for Systems Neuroscience at Washington University. Extensive editing of both the content and the language was performed by Rhoda E. and Edmund F. Perozzi. Funding to pay the Open Access publication charges for this article was provided by the Natural Science Foundation of China (Grant No. 91432302). *Conflict of Interest*: The authors declare that the research was conducted in the absence of any commercial or financial relationships that could be construed as a potential conflict of interest.

References

Alexander-Bloch A, Giedd JN, Bullmore E. 2013. Imaging structural co-variance between human brain regions. Nat Rev Neurosci. 14:322–336.

Amunts K, Hawrylycz MJ, Van Essen DC, Van Horn JD, Harel N, Poline JB, De Martino F, Bjaalie JG, Dehaene-Lambertz G, Dehaene S, et al. 2014. Interoperable atlases of the human brain. Neuroimage. 99:525–532.

Amunts K, Lenzen M, Friederici AD, Schleicher A, Morosan P, Palomero-Gallagher N, Zilles K. 2010. Broca's region: novel

organizational principles and multiple receptor mapping. PLoS Biol. 8:e1000489.
Amunts K, Zilles K. 2015. Architectonic mapping of the human brain beyond Brodmann. Neuron. 88:1086–1107.
Anwander A, Tittgemeyer M, von Cramon DY, Friederici AD, Knosche TR. 2007. Connectivity-based parcellation of Broca's area. Cereb Cortex. 17:816–825.
Barbas H. 2015. General cortical and special prefrontal connections: principles from structure to function. Annu Rev Neurosci. 38:269–289.
Barbas H, Rempel-Clower N. 1997. Cortical structure predicts the pattern of corticocortical connections. Cereb Cortex. 7:635–646.
Barnes KA, Nelson SM, Cohen AL, Power JD, Coalson RS, Miezin FM, Vogel AC, Dubis JW, Church JA, Petersen SE, et al. 2011. Parcellation in left lateral parietal cortex is similar in adults and children. Cereb Cortex. 22:1148–1158.
Beckmann M, Johansen-Berg H, Rushworth MF. 2009. Connectivity-based parcellation of human cingulate cortex and its relation to functional specialization. J Neurosci. 29: 1175–1190.
Behrens TE, Berg HJ, Jbabdi S, Rushworth MF, Woolrich MW. 2007. Probabilistic diffusion tractography with multiple fibre orientations: what can we gain? Neuroimage. 34:144–155.
Behrens TE, Johansen-Berg H, Woolrich MW, Smith SM, Wheeler-Kingshott CA, Boulby PA, Barker GJ, Sillery EL, Sheehan K, Ciccarelli O, et al. 2003. Non-invasive mapping of connections between human thalamus and cortex using diffusion imaging. Nat Neurosci. 6:750–757.
Bludau S, Eickhoff SB, Mohlberg H, Caspers S, Laird AR, Fox PT, Schleicher A, Zilles K, Amunts K. 2014. Cytoarchitecture, probability maps and functions of the human frontal pole. Neuroimage. 93(Pt 2):260–275.
Bohland JW, Bokil H, Allen CB, Mitra PP. 2009. The brain atlas concordance problem: quantitative comparison of anatomical parcellations. PLoS ONE. 4:e7200.
Brett M, Johnsrude IS, Owen AM. 2002. The problem of functional localization in the human brain. Nat Rev Neurosci. 3:243–249.
Brodmann K. 1909. Vergleichende Lokalisationslehre der Großhirnrinde in ihren Prinzipien dargestellt auf Grund des Zellenbaues. Leipzig, Germany: von Johann Ambrosius Barth.
Caspers S, Eickhoff SB, Geyer S, Scheperjans F, Mohlberg H, Zilles K, Amunts K. 2008. The human inferior parietal lobule in stereotaxic space. Brain Struct Funct. 212:481–495.
Cauda F, Vercelli A. 2013. How many clusters in the insular cortex? Cereb Cortex. 23:2779–2780.
Chang LJ, Yarkoni T, Khaw MW, Sanfey AG. 2013. Decoding the role of the insula in human cognition: functional parcellation and large-scale reverse inference. Cereb Cortex. 23:739–749.
Cieslik EC, Zilles K, Caspers S, Roski C, Kellermann TS, Jakobs O, Langner R, Laird AR, Fox PT, Eickhoff SB. 2013. Is there "one" DLPFC in cognitive action control? Evidence for heterogeneity from co-activation-based parcellation. Cereb Cortex. 23:2677–2689.
Clos M, Amunts K, Laird AR, Fox PT, Eickhoff SB. 2013. Tackling the multifunctional nature of Broca's region meta-analytically: co-activation-based parcellation of area 44. Neuroimage. 83:174–188.
Cohen AL, Fair DA, Dosenbach NU, Miezin FM, Dierker D, Van Essen DC, Schlaggar BL, Petersen SE. 2008. Defining functional areas in individual human brains using resting functional connectivity MRI. Neuroimage. 41:45–57.
Cohen MX, Lombardo MV, Blumenfeld RS. 2008. Covariance-based subdivision of the human striatum using T1-weighted MRI. Eur J Neurosci. 27:1534–1546.
Craddock RC, James GA, Holtzheimer PE III, Hu XP, Mayberg HS. 2012. A whole brain fMRI atlas generated via spatially constrained spectral clustering. Hum Brain Mapp. 33:1914–1928.
Cui Y, Liu B, Zhou Y, Fan L, Li J, Zhang Y, Wu H, Hou B, Wang C, Zheng F, et al. 2015. Genetic effects on fine-grained human cortical regionalization. Cereb Cortex. doi: 10.1093/cercor/bhv176.
de Reus MA, van den Heuvel MP. 2013. The parcellation-based connectome: limitations and extensions. Neuroimage. 80: 397–404.
Desikan RS, Segonne F, Fischl B, Quinn BT, Dickerson BC, Blacker D, Buckner RL, Dale AM, Maguire RP, Hyman BT, et al. 2006. An automated labeling system for subdividing the human cerebral cortex on MRI scans into gyral based regions of interest. NeuroImage. 31:968–980.
Devlin JT, Poldrack RA. 2007. In praise of tedious anatomy. NeuroImage. 37:1033–1041; discussion 1050–1038.
Eickhoff SB, Bzdok D, Laird AR, Roski C, Caspers S, Zilles K, Fox PT. 2011. Co-activation patterns distinguish cortical modules, their connectivity and functional differentiation. Neuroimage. 57:938–949.
Eickhoff SB, Grefkes C. 2011. Approaches for the integrated analysis of structure, function and connectivity of the human brain. Clin EEG Neurosci. 42:107–121.
Eickhoff SB, Jbabdi S, Caspers S, Laird AR, Fox PT, Zilles K, Behrens TE. 2010. Anatomical and functional connectivity of cytoarchitectonic areas within the human parietal operculum. J Neurosci. 30:6409–6421.
Eickhoff SB, Stephan KE, Mohlberg H, Grefkes C, Fink GR, Amunts K, Zilles K. 2005. A new SPM toolbox for combining probabilistic cytoarchitectonic maps and functional imaging data. NeuroImage. 25:1325–1335.
Eickhoff SB, Thirion B, Varoquaux G, Bzdok D. 2015. Connectivity-based parcellation: critique and implications. Hum Brain Mapp. doi:10.1002/hbm.22933.
Evans AC, Janke AL, Collins DL, Baillet S. 2012. Brain templates and atlases. NeuroImage. 62:911–922.
Fan L, Wang J, Zhang Y, Han W, Yu C, Jiang T. 2014. Connectivity-based parcellation of the human temporal pole using diffusion tensor imaging. Cereb Cortex. 24:3365–3378.
Felleman DJ, Van Essen DC. 1991. Distributed hierarchical processing in the primate cerebral cortex. Cereb Cortex. 1:1–47.
Fonov V, Evans AC, Botteron K, Almli CR, McKinstry RC, Collins DL, Grp BDC. 2011. Unbiased average age-appropriate atlases for pediatric studies. NeuroImage. 54:313–327.
Fox PT, Lancaster JL, Laird AR, Eickhoff SB. 2014. Meta-analysis in human neuroimaging: computational modeling of large-scale databases. Annu Rev Neurosci. 37:409–434.
Glasser MF, Sotiropoulos SN, Wilson JA, Coalson TS, Fischl B, Andersson JL, Xu J, Jbabdi S, Webster M, Polimeni JR, et al. 2013. The minimal preprocessing pipelines for the Human Connectome Project. NeuroImage. 80:105–124.
Glickfeld LL, Andermann ML, Bonin V, Reid RC. 2013. Cortico-cortical projections in mouse visual cortex are functionally target specific. Nat Neurosci. 16; doi:10.1038/nn.3300.
Gong G, He Y, Concha L, Lebel C, Gross DW, Evans AC, Beaulieu C. 2009. Mapping anatomical connectivity patterns of human cerebral cortex using in vivo diffusion tensor imaging tractography. Cereb Cortex. 19:524–536.
Gordon EM, Laumann TO, Adeyemo B, Huckins JF, Kelley WM, Petersen SE. 2016. Generation and evaluation of a cortical area parcellation from resting-state correlations. Cereb Cortex. 26:288–303.

Gutman B, Leonardo C, Jahanshad N, Hibar D, Eschenburg K, Nir T, Villalon J, Thompson P. 2014. Registering cortical surfaces based on whole-brain structural connectivity and continuous connectivity analysis. Med Image Comput Comput Assist Interv. 17:161–168.

Heiervang E, Behrens TE, Mackay CE, Robson MD, Johansen-Berg H. 2006. Between session reproducibility and between subject variability of diffusion MR and tractography measures. NeuroImage. 33:867–877.

Hilgetag CC, Grant S. 2010. Cytoarchitectural differences are a key determinant of laminar projection origins in the visual cortex. NeuroImage. 51:1006–1017.

Honey CJ, Sporns O, Cammoun L, Gigandet X, Thiran JP, Meuli R, Hagmann P. 2009. Predicting human resting-state functional connectivity from structural connectivity. Proc Natl Acad Sci USA. 106:2035–2040.

Jbabdi S, Sotiropoulos SN, Haber SN, Van Essen DC, Behrens TE. 2015. Measuring macroscopic brain connections in vivo. Nat Neurosci. 18:1546–1555.

Jenkinson M, Bannister P, Brady M, Smith S. 2002. Improved optimization for the robust and accurate linear registration and motion correction of brain images. NeuroImage. 17:825–841.

Jenkinson M, Beckmann CF, Behrens TE, Woolrich MW, Smith SM. 2012. Fsl. NeuroImage. 62:782–790.

Jiang T. 2013. Brainnetome: a new -ome to understand the brain and its disorders. NeuroImage. 80:263–272.

Johansen-Berg H, Behrens TE, Robson MD, Drobnjak I, Rushworth MF, Brady JM, Smith SM, Higham DJ, Matthews PM. 2004. Changes in connectivity profiles define functionally distinct regions in human medial frontal cortex. Proc Natl Acad Sci USA. 101:13335–13340.

Johansen-Berg H, Della-Maggiore V, Behrens TE, Smith SM, Paus T. 2007. Integrity of white matter in the corpus callosum correlates with bimanual co-ordination skills. NeuroImage. 36 (Suppl. 2):T16–T21.

Kelly C, Toro R, Di Martino A, Cox CL, Bellec P, Castellanos FX, Milham MP. 2012. A convergent functional architecture of the insula emerges across imaging modalities. NeuroImage. 61:1129–1142.

Kim J-H, Lee J-M, Jo HJ, Kim SH, Lee JH, Kim ST, Seo SW, Cox RW, Na DL, Kim SI, et al. 2010. Defining functional SMA and pre-SMA subregions in human MFC using resting state fMRI: functional connectivity-based parcellation method. NeuroImage. 49:2375.

Klein JC, Behrens TE, Robson MD, Mackay CE, Higham DJ, Johansen-Berg H. 2007. Connectivity-based parcellation of human cortex using diffusion MRI: establishing reproducibility, validity and observer independence in BA 44/45 and SMA/pre-SMA. NeuroImage. 34:204–211.

Kurth F, Eickhoff SB, Schleicher A, Hoemke L, Zilles K, Amunts K. 2010. Cytoarchitecture and probabilistic maps of the human posterior insular cortex. Cereb Cortex. 20:1448–1461.

Kurth F, Zilles K, Fox PT, Laird AR, Eickhoff SB. 2010. A link between the systems: functional differentiation and integration within the human insula revealed by meta-analysis. Brain Struct Funct. 214:519–534.

Laird AR, Eickhoff SB, Fox PM, Uecker AM, Ray KL, Saenz JJ Jr, McKay DR, Bzdok D, Laird RW, Robinson JL, et al. 2011. The BrainMap strategy for standardization, sharing, and meta-analysis of neuroimaging data. BMC Res Notes. 4:349.

Laird AR, Eickhoff SB, Kurth F, Fox PM, Uecker AM, Turner JA, Robinson JL, Lancaster JL, Fox PT. 2009. ALE meta-analysis workflows via the brainmap database: progress towards a probabilistic functional brain atlas. Front Neuroinform. 3:23.

Laumann Timothy O, Gordon Evan M, Adeyemo B, Snyder Abraham Z, Joo Sung J, Chen M-Y, Gilmore Adrian W, McDermott Kathleen B, Nelson Steven M, Dosenbach Nico UF, et al. 2015. Functional system and areal organization of a highly sampled individual human brain. Neuron. 87:657–670.

Lefranc S, Roca P, Perrot M, Poupon C, Le Bihan D, Mangin JF, Riviere D. 2016. Groupwise connectivity-based parcellation of the whole human cortical surface using watershed-driven dimension reduction. Med Image Anal. 30:11–29.

Liu H, Qin W, Li W, Fan L, Wang J, Jiang T, Yu C. 2013. Connectivity-based parcellation of the human frontal pole with diffusion tensor imaging. J Neurosci. 33:6782–6790.

Liu H, Qin W, Qi H, Jiang T, Yu C. 2015. Parcellation of the human orbitofrontal cortex based on gray matter volume covariance. Hum Brain Mapp. 36:538–548.

Makuuchi M, Bahlmann J, Anwander A, Friederici AD. 2009. Segregating the core computational faculty of human language from working memory. Proc Natl Acad Sci USA. 106:8362–8367.

Mechelli A, Friston KJ, Frackowiak RS, Price CJ. 2005. Structural covariance in the human cortex. J Neurosci. 25:8303–8310.

Morel A, Gallay MN, Baechler A, Wyss M, Gallay DS. 2013. The human insula: architectonic organization and postmortem MRI registration. Neuroscience. 236:117–135.

Moreno-Dominguez D, Anwander A, Knösche TR. 2014. A hierarchical method for whole-brain connectivity-based parcellation. Hum Brain Mapp. 35:5000–5025.

Muhle-Karbe PS, Derrfuss J, Lynn MT, Neubert FX, Fox PT, Brass M, Eickhoff SB. 2015. Co-activation-based parcellation of the lateral prefrontal cortex delineates the inferior frontal junction area. Cereb Cortex. doi:10.1093/cercor/bhv073.

Munkres J. 1957. Algorithms for the assignment and transportation problems. J Soc Ind Appl Math. 5:32–38.

Nelson SM, Cohen AL, Power JD, Wig GS, Miezin FM, Wheeler ME, Velanova K, Donaldson DI, Phillips JS, Schlaggar BL, et al. 2010. A parcellation scheme for human left lateral parietal cortex. Neuron. 67:156–170.

Neubert FX, Mars RB, Thomas AG, Sallet J, Rushworth MF. 2014. Comparison of human ventral frontal cortex areas for cognitive control and language with areas in monkey frontal cortex. Neuron. 81:700–713.

Ongur D, Ferry AT, Price JL. 2003. Architectonic subdivision of the human orbital and medial prefrontal cortex. J Comp Neurol. 460:425–449.

Palomero-Gallagher N, Eickhoff SB, Hoffstaedter F, Schleicher A, Mohlberg H, Vogt BA, Amunts K, Zilles K. 2015. Functional organization of human subgenual cortical areas: relationship between architectonical segregation and connectional heterogeneity. NeuroImage. 115:177–190.

Passingham RE, Stephan KE, Kotter R. 2002. The anatomical basis of functional localization in the cortex. Nat Rev Neurosci. 3:606–616.

Petrides M, Pandya DN. 2002. Comparative cytoarchitectonic analysis of the human and the macaque ventrolateral prefrontal cortex and corticocortical connection patterns in the monkey. Eur J Neurosci. 16:291–310.

Petrides M, Pandya DN. 1999. Dorsolateral prefrontal cortex: comparative cytoarchitectonic analysis in the human and the macaque brain and corticocortical connection patterns. Eur J Neurosci. 11:1011–1036.

Rempel-Clower NL, Barbas H. 2000. The laminar pattern of connections between prefrontal and anterior temporal cortices in the rhesus monkey is related to cortical structure and function. Cereb Cortex. 10:851–865.

Richiardi J, Altmann A, Milazzo A-C, Chang C, Chakravarty MM, Banaschewski T, Barker GJ, Bokde ALW, Bromberg U, Büchel C, et al. 2015. Correlated gene expression supports synchronous activity in brain networks. Science. 348:1241–1244.

Saygin ZM, Osher DE, Koldewyn K, Reynolds G, Gabrieli JD, Saxe RR. 2012. Anatomical connectivity patterns predict face selectivity in the fusiform gyrus. Nat Neurosci. 15:321–327.

Scannell JW, Blakemore C, Young MP. 1995. Analysis of connectivity in the cat cerebral cortex. J Neurosci. 15:1463–1483.

Scheperjans F, Hermann K, Eickhoff SB, Amunts K, Schleicher A, Zilles K. 2008. Observer-independent cytoarchitectonic mapping of the human superior parietal cortex. Cereb Cortex. 18:846–867.

Scholtens LH, Schmidt R, de Reus MA, van den Heuvel MP. 2014. Linking macroscale graph analytical organization to microscale neuroarchitectonics in the macaque connectome. J Neurosci. 34:12192–12205.

Smith SM, Beckmann CF, Andersson J, Auerbach EJ, Bijsterbosch J, Douaud G, Duff E, Feinberg DA, Griffanti L, Harms MP, et al. 2013. Resting-state fMRI in the Human Connectome Project. NeuroImage. 80:144–168.

Sporns O. 2015. Cerebral cartography and connectomics. Philos Trans R Soc Lond B Biol Sci. 370; doi:10.1098/rstb.2014.0173.

Toga AW, Thompson PM, Mori S, Amunts K, Zilles K. 2006. Towards multimodal atlases of the human brain. Nat Rev Neurosci. 7:952–966.

Tungaraza RL, Mehta SH, Haynor DR, Grabowski TJ. 2015. Anatomically informed metrics for connectivity-based cortical parcellation from diffusion MRI. IEEE J Biomed Health Inform. 19:1375–1383.

Tziortzi AC, Haber SN, Searle GE, Tsoumpas C, Long CJ, Shotbolt P, Douaud G, Jbabdi S, Behrens TE, Rabiner EA, et al. 2014. Connectivity-based functional analysis of dopamine release in the striatum using diffusion-weighted MRI and positron emission tomography. Cereb Cortex. 24:1165–1177.

Tzourio-Mazoyer N, Landeau B, Papathanassiou D, Crivello F, Etard O, Delcroix N, Mazoyer B, Joliot M. 2002. Automated anatomical labeling of activations in SPM using a macroscopic anatomical parcellation of the MNI MRI single-subject brain. NeuroImage. 15:273–289.

van den Heuvel MP, Mandl RC, Kahn RS, Hulshoff Pol HE. 2009. Functionally linked resting-state networks reflect the underlying structural connectivity architecture of the human brain. Hum Brain Mapp. 30:3127–3141.

van den Heuvel MP, Scholtens LH, Feldman Barrett L, Hilgetag CC, de Reus MA. 2015. Bridging cytoarchitectonics and connectomics in human cerebral cortex. J Neurosci. 35:13943–13948.

Van Essen DC. 2013. Cartography and connectomes. Neuron. 80:775–790.

Van Essen DC, Smith SM, Barch DM, Behrens TE, Yacoub E, Ugurbil K, Consortium WU-MH. 2013. The WU-Minn Human Connectome Project: an overview. NeuroImage. 80:62–79.

Vogt BA, Nimchinsky EA, Vogt LJ, Hof PR. 1995. Human cingulate cortex: surface features, flat maps, and cytoarchitecture. J Comp Neurol. 359:490–506.

Von Economo CF, Koskinas GN. 1925. Die Cytoarchitektonik der Hirnrinde des erwachsenen Menschen. Berlin: Springer.

Wang J, Fan L, Zhang Y, Liu Y, Jiang D, Zhang Y, Yu C, Jiang T. 2012. Tractography-based parcellation of the human left inferior parietal lobule. NeuroImage. 63:641–652.

Wang J, Yang Y, Fan L, Xu J, Li C, Liu Y, Fox PT, Eickhoff SB, Yu C, Jiang T. 2015. Convergent functional architecture of the superior parietal lobule unraveled with multimodal neuroimaging approaches. Hum Brain Mapp. 36:238–257.

Wang Q, Yap PT, Wu G, Shen D. 2014. Diffusion tensor image registration using hybrid connectivity and tensor features. Hum Brain Mapp. 35:3529–3546.

Wig GS, Laumann TO, Petersen SE. 2014. An approach for parcellating human cortical areas using resting-state correlations. NeuroImage. 93(Part. 2):276–291.

Yang Y, Fan L, Chu C, Zhuo J, Wang J, Fox PT, Eickhoff SB, Jiang T. 2015. Identifying functional subdivisions in the human brain using meta-analytic activation modeling-based parcellation. Neuroimage. 124:300–309.

Zhang Y, Caspers S, Fan L, Fan Y, Song M, Liu C, Mo Y, Roski C, Eickhoff S, Amunts K, et al. 2015. Robust brain parcellation using sparse representation on resting-state fMRI. Brain Struct Funct. 220:3565–3579.

Zhuo J, Fan L, Liu Y, Zhang Y, Yu C, Jiang T. 2016. Connectivity profiles reveal a transition subarea in the parahippocampal region that integrates the anterior temporal-posterior medial systems. J Neurosci. 36:2782–2795.

Zilles K, Amunts K. 2010. Centenary of Brodmann's map—conception and fate. Nat Rev Neurosci. 11:139–145.